Journal of Non-Newtonian Fluid Mechanics 322 (2023) 105151

Contents lists available at ScienceDirect

Journal of Non-Newtonian Fluid Mechanics

journal homepage: www.elsevier.com/locate/jnnfm

Designing a swimming rheometer to measure the linear and non-linear properties of a viscoelastic fluid

Boon Siong Neo [a], Eric S.G. Shaqfeh [a,b,*]

[a] Department of Chemical Engineering, Stanford University, Stanford, 94305, CA, USA
[b] Department of Mechanical Engineering, Stanford University, Stanford, 94305, CA, USA

ARTICLE INFO

MSC:
0000
1111

Keywords:
Propulsion
Viscoelasticity
Swimmer
Giesekus fluid
Normal stresses

ABSTRACT

At low Reynolds numbers, "swirlers" – swimmers with an axisymmetric "head" and "tail" counterrotating about the axis of symmetry – generate no net propulsion in a Newtonian fluid as a consequence of the "scallop theorem". Viscoelasticity in the suspending fluid breaks the time-reversibility and allows swirlers to propel themselves, with the swim speed being a function of swimmer geometry, fluid elasticity, and swimming gait. Using analytical theory and numerical simulations, we study the unsteady motion of a freely-suspended self-propelled swirler though viscoelastic fluids described by the Giesekus model, allowing for general axisymmetric geometry and time-dependent tail rotation rate. We show the steady swim speed can be calculated for general arbitrary axisymmetric geometries at low Deborah number via the reciprocal theorem and the solution of two Newtonian flow problems. In this "weak flow" limit, we analytically determine the swim speed and its dependence on the parameters of the Giesekus fluid which in turn are related to the primary and secondary normal stress coefficients Ψ_1 and Ψ_2. Furthermore, at low De, we derive the unsteady swim speed as a function of a specified unsteady tail rotation rate and the material properties of the suspending fluid. We show that for a particular tail rotation rate, the unsteady swim speed can be analyzed to recover the spectrum of fluid relaxation times, analogous to small-amplitude oscillatory shear measurements on a benchtop rheometer. This study expands upon the design space for a "swimming rheometer" by increasing its functionality to make and interpret rheological measurements.

1. Introduction

Microscopic organisms swim through viscous fluids in a regime where the Reynolds number is virtually zero [1,2]. In this regime and with a Newtonian fluid, only specific swimmer gaits allow for translation [1]. For instance, any swim stroke involving reciprocal, or time-reversible, motion, creates no propulsion because the Stokes equations, which govern the flow in this regime, are linear [2]: the time-reversible motion creates a time-reversible force on the swimmer, such that the net propulsion over a complete swim stroke is zero. More generally, this applies when the swimmer configuration or shape changes reversibly over the course of the entire stroke, regardless of the rate at which these shape changes occur [3], due to the quasi-steady nature of the Stokes equations.

However, if the fluid is non-Newtonian, the linearity of the equations that govern the flow is broken, and propulsion, even with time-reversible motion, becomes possible. These include non-elastic effects (i.e. in the absence of normal stresses); for example, a miniature scallop, either externally actuated by magnetic fields [4,5] or by an on-board motor [4], was designed to swim in a shear-thickening or shear-thinning fluid via employing different opening and closing rates to create different shear rates, varying viscosity, and hence asymmetric propulsion over its reciprocal stroke. Viscoelasticity in the suspending fluid also creates asymmetric propulsion for these scallop swimmers [6], with the propulsion created by unsteady normal stresses (tension along streamlines due to stretched polymers) where propulsion is created even if the opening and closing rates are the same.

Two-sphere swimmer models have served as a useful starting point for mathematical analysis, due to the extensive literature available for flows around spherical particles. One such example for which the combination of fore-aft asymmetry and viscoelasticity enables propulsion is the oscillating two-sphere swimmer: two spheres of different sizes a fixed distance apart rigidly oscillated by an external force back-and-forth along the axis connecting their two centers [7], or connected by an infinitesimally thin rod that expands and contracts such that its length varies sinusoidally in time [7–9]. The authors adopted a combination of perturbation theory (perturbing either the domain

* Corresponding author.
E-mail addresses: neobs@stanford.edu (B.S. Neo), esgs@stanford.edu (E.S.G. Shaqfeh).

https://doi.org/10.1016/j.jnnfm.2023.105151
Received 10 August 2023; Received in revised form 10 November 2023; Accepted 11 November 2023
Available online 13 November 2023

boundary [7] or the fluid elasticity [9]) and the reciprocal theorem to derive the time-averaged swim speed over a period of oscillation, and show that it is non-monotonic in the Deborah number. For the expanding-contracting oscillating swimmer, the authors showed that propulsion arises from an imbalance in the force required to expand, versus to contract, the swimmer, over the course of a reciprocal stroke.

Two-sphere swimmers with a gait where the spheres rotate have also been studied for propulsion created when viscoelasticity breaks the symmetry of Stokes equations. A single sphere rotating in a viscoelastic fluid can propel along the axis of rotation if the fore-aft symmetry of the sphere about the equatorial plane is broken, e.g. by the application of a symmetry-breaking static magnetic field [10]. The addition of a second sphere, with its center placed along the rotation axis of the first and rotating about the same axis, can break this fore-aft symmetry and enable propulsion in a viscoelastic fluid; this motion creates no propulsion in Newtonian fluids due to a combination of kinematic reversibility and reflection symmetry [11]. Two-sphere swimmers rigidly rotating along their axis of symmetry ("swirling") under an external applied torque [11,12] were found to propel along their axis of symmetry, with speed being a function of the size ratio of the spheres. Another experimental study showed that a "microsnowman" – two bonded spheres rotated by an applied magnetic field – swim in synthetic mucus, with approximately linear speed over a range of small rotation rates [13]. In contrast to these rigidly-rotated two-sphere swimmers, freely-suspended two-sphere swirlers were also studied, where the spheres counter-rotate and there is no net torque [14,15]. Such swirlers are propelled via non-zero normal stresses in elastic fluids [11,14], making their translational velocity a measure of the elastic normal stresses. In all cases, the propulsion speed is a function of not only the swimmer geometry and gait, but also the material properties of the fluid — its elasticity. Thus, an artificial swimmer can be designed to move with a prescribed gait, and its velocity analyzed to determine fluid properties — a "swimming rheometer".

Experiments recently completed with a freely-suspended robotic swirler [15] were a first step towards designing and fabricating such a rheometer. This autonomous sensor has the potential to make rheological measurements of fluids *in situ*, allowing for measurements of the fluid in its operating conditions e.g. as a process rheometer.

Inspired by transient tests performed on benchtop rheometers (e.g. small-amplitude oscillatory shear, stress relaxation), we consider the case where the swirler rotation rate varies with time. Previous studies with swimmer configurations or velocity boundary conditions that were periodic in time evaluated the time-averaged equations over the swim stroke [6,7,9], or by making use of the Fourier representation and working with the complex viscosity [8]. For single spheres in viscoelastic fluids, previous studies focused on translation [16] and steady rotation [17], and unsteady flow studies looked at settling [18], translation [19] and simultaneous translation and rotation [20]; the latter two studies also work with the complex viscosity in the Fourier domain to establish the time-dependence. Working with the complex viscosity allows the introduction of arbitrary time-dependence in the velocity boundary conditions, and we adopt a similar approach in our study, leaving our expression in terms of a convolution in the time-domain Appendix C.

In this work, we extend the previous analysis to freely-suspended axisymmetric swirlers, where the tail rotation rate can vary with time. We show that the velocity of a steady swirler for a fixed tail rotation rate, which is a measure of normal stresses in the fluid, can be predicted (over a range of small Deborah number) for various swirler geometries if Newtonian solutions to two other problems with the same geometry are known. We derive a relation between a time-varying tail rotation rate, and the translational velocity of the freely-suspended swirler. We show that for a certain functional form of the tail rotation rate, the swirler's translational velocity can be analyzed to obtain the linear viscoelasticity of the suspending fluid, analogous to small amplitude oscillatory shear experiments on a benchtop rheometer. To do this, we first use a combination of perturbation theory and the reciprocal theorem (Sections 2.1–2.4) to get analytical predictions of the swimmer's velocity. We then conduct fully-resolved numerical simulations (Section 2.5) to compare the results against our theoretical predictions, and show how we can analyze the simulation results to recover the linear viscoelastic properties of the suspending fluid. The calculations presented in this paper are valid for general weakly elastic fluids (i.e. the general second order fluid [21]), for axisymmetric swirler geometries with prescribed rotation rates, even if they move under an applied torque.

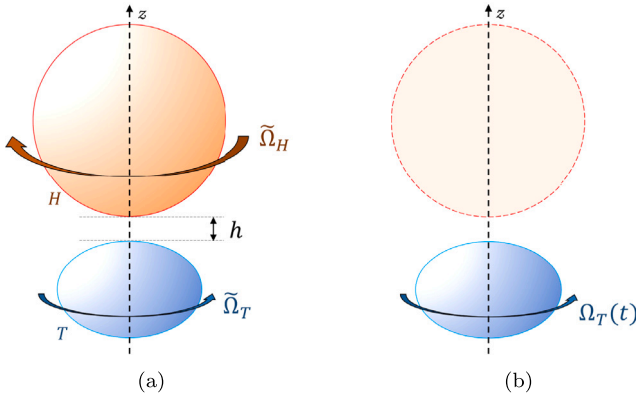

Fig. 1. Depiction of freely-suspended swirler geometry. (a) Tail T has characteristic rotation rate $\tilde{\Omega}_T$ specified; head H characteristic rotation rate $\tilde{\Omega}_H$ is opposite in direction to counter the tail torque. The head and tail area separated by some distance h. (b) We initially consider the fields created by a single rigidly-rotating "tail" with time-varying rotation rate $\Omega_T(t)$, and subsequently consider the effect of the head.

2. Methods

2.1. Governing equations

The fluid surrounding the swirling microswimmer is described mathematically by conservation of momentum and mass, with the equations rescaled to dimensionless form by a careful choice of scale factors. Fig. 1 illustrates the swimmer geometry: two rotating bodies of revolution, with one as the "head" and the other as the "tail". Their bodies are arranged coaxially and they are not physically connected, but maintained at some distance h.[1] They rotate along their axis of shape revolution; without loss of generality, we adopt the reference frame where this is the z-axis (equivalently the x_3-axis), pointing from the "tail" to the "head". Due to the axisymmetric geometry and rotation about the symmetry axis, its translational velocity is constrained to lie along this axis as well. Since the swimmer is in general freely-suspended, we will prescribe the tail rotation rate $\Omega_T(t)$ and have the head rotation $\Omega_H(t)$ be determined from the torque-free condition. We define the characteristic rate of rotation to be $\tilde{\Omega}_T$ — for example, when the tail rotation rate is oscillating at some frequency about the mean value, $\tilde{\Omega}_T$ is the mean rotation rate. Since the head and tail can be of arbitrary axisymmetric geometries, we consider their hydrodynamic torque in a Newtonian fluid at Re = 0 and use it to define characteristic length scales:

$$L_i^H = 8\pi\eta_0 l_H^3 \tilde{\Omega}_H \delta_{i3} \tag{1}$$

$$L_i^T = 8\pi\eta_0 l_T^3 \tilde{\Omega}_T \delta_{i3} \tag{2}$$

For arbitrary geometries, the direction of propulsion is unknown; Binagia and Shaqfeh [14] propose that propulsion in the direction of the object identified as the 'head' occurs when $D_H l_H^4 / D_T l_T^4 > 1$,

[1] This has been achieved experimentally [15].

where D_H, D_T are the drag coefficients of the head and tail respectively translating through a Newtonian fluid along their axis of symmetry.

The characteristic viscous stress scale is $\eta_0\tilde{\Omega}_T$, where η_0 is the zero shear viscosity of the fluid. We will assume the swimmer motion is such that the Reynolds number $\mathrm{Re} \equiv \frac{\rho\tilde{\Omega}_T l_c}{\eta_0}$ – where l_c is either l_H or l_T – of the flow is in the Stokes regime, as with biological microswimmers [22]. Thus we use the dimensionless Stokes equations for an incompressible fluid:

$$\nabla_j \sigma_{ij}^{total} = 0 \tag{3}$$

$$\nabla_i u_i = 0 \tag{4}$$

where u_i is the velocity field in the fluid made dimensionless by l_c, and $\sigma_{ij}^{\mathrm{total}}$ is the Cauchy or total stress made dimensionless by $\eta_0\tilde{\Omega}_T$

To incorporate viscoelasticity, we assume the total stress $\sigma_{ij}^{\mathrm{total}}$ arises from the sum of a Newtonian and polymeric contribution:

$$\sigma_{ij}^{total} = -p\delta_{ij} + 2\beta E_{ij} + (1-\beta)\sigma_{ij}^{p} \tag{5}$$

$$E_{ij} = \frac{1}{2}\left(\nabla_j u_i + \nabla_i u_j\right) \tag{6}$$

where p is the (solvent) pressure made dimensionless by $\eta_0\tilde{\Omega}_T$; σ_{ij}^p is the stress arising from polymer molecules in the fluid made dimensionless by $\eta_p\tilde{\Omega}_T$; and $\beta \equiv \frac{\eta_s}{\eta_s+\eta_p}$ is the solvent viscosity over the zero-shear viscosity. To describe σ_{ij}^p we will start with the Oldroyd-B and Giesekus constitutive equations, which are derived from treating polymer molecules as Hookean dumbbells. However, many of our results will be for the general second-order fluid (e.g. the low De expansion of the Giesekus equation [23]) and therefore of broader generality [21]. The nondimensional constitutive evolution equation is as follows:

$$\frac{\partial\sigma_{ij}^p}{\partial t} + \mathrm{De}\left(u_k\nabla_k\sigma_{ij}^p - \nabla_k u_i\sigma_{jk}^p - \nabla_k u_j\sigma_{ik}^p + \alpha\sigma_{ik}^p\sigma_{kj}^p\right) + \sigma_{ij}^p = 2E_{ij} \tag{7}$$

where time is non-dimensionalized by the polymer relaxation time λ. The Deborah number $\mathrm{De} \equiv \lambda\tilde{\Omega}_T$ is a measure of fluid elasticity. The Giesekus mobility parameter α reflects the effect of anisotropic drag on the polymer molecule as it stretches, and non-zero values lead to predictions of shear-thinning and non-zero second normal stress differences [21]. When $\alpha = 0$, the Oldroyd-B model [24] is recovered. This nondimensionalization resembles that carried out by Joens and Swan [19], in which the characteristic timescale for the unsteady term differs from that of the remaining terms arising from the upper convected derivative. In their work, they note that "the imposed flow can change with arbitrary rapidity", thus the unsteady term persists even at small Deborah numbers. Our choice of timescale, which is appropriate for investigating linear viscoelastic behavior, leads to the same retention of the unsteady term in the limit as $\mathrm{De} \to 0$

2.2. Perturbation theory

The effect of weak elasticity is analyzed through perturbation theory, in a method similar to previous studies of bodies in elastic fluids [19,23]. For small Deborah number, we suppose the dimensionless variables can be written as a power series as follows:

$$p = p^{(0)} + \mathrm{De}\, p^{(1)} + \cdots \tag{8}$$

$$u_i = u_i^{(0)} + \mathrm{De}\, u_i^{(1)} + \cdots \tag{9}$$

$$\sigma_{ij}^p = \sigma_{ij}^{p(0)} + \mathrm{De}\, \sigma_{ij}^{p(1)} + \cdots \tag{10}$$

To determine the solution for the freely suspended swimmer, we first consider the problem of an arbitrary axisymmetric body swirling in an unbounded viscoelastic fluid domain; one could think of this as first focusing on just the "tail" rotating without the "head" (as depicted in Fig. 1(b)). This gives the following boundary conditions:

$$p(r \to \infty) \to 0 \tag{11}$$

$$u_i(x_i^s) = \epsilon_{ijk}\Omega(t)\delta_{j3}x_k^s \qquad \forall\, x_i^s \text{ on surface} \tag{12}$$

$$u_i(|x_i| \to \infty) \to 0 \tag{13}$$

The rotation rate can have a general time-dependence; however we first provide a derivation for the case where the rotation rate is sinusoidal with time around a mean offset, i.e. $\Omega(t) = 1 + \varepsilon\cos\omega t = \Re\{1 + \varepsilon e^{i\omega t}\}$; we work with the complex representation to simplify the algebra. The frequency, ω, is non-dimensionalized by the polymer relaxation time λ. The amplitude of the oscillation is small compared to its mean, i.e. $\varepsilon \ll 1$. We are interested in the long-time behavior of the pressure, velocity, and polymer stress fields, as they dictate the propulsion and hence translational velocity of the swimmer — the primary measure of interest. As we demonstrate below, the swirler adopts a speed which oscillates about a mean value. The ratio of the oscillation amplitudes to the mean speed reflects the relaxation time spectrum of the fluid, from which the dimensionless complex modulus or complex viscosity can be obtained.

2.2.1. Zero-th order solution for pressure, velocity, and polymer stress

At zero-th order, the governing equations and boundary conditions are as follows:

$$0 = -\nabla_i p^{(0)} + \beta\nabla^2 u_i^{(0)} + (1-\beta)\nabla_j\sigma_{ij}^{p(0)} \tag{14}$$

$$\nabla_i u_i^{(0)} = 0 \tag{15}$$

$$\frac{\partial\sigma_{ij}^{p(0)}}{\partial t} + \sigma_{ij}^{p(0)} = 2E_{ij}^{(0)} \tag{16}$$

$$u_i^{(0)}|_{\mathrm{surface}} = (1 + \varepsilon e^{i\omega t})\epsilon_{ijk}\delta_{j3}x_k^s \qquad \forall\, x_i^s \text{ on surface} \tag{17}$$

We assume the variables are separable into the product of spatial and time dependent functions, with the spatially-varying components denoted by overbars. From the velocity boundary condition, the zero-th order velocity, and subsequently polymer stress, can be determined:

$$u_i^{(0)} = (1 + \varepsilon e^{i\omega t})\bar{u}_i^{(0)} \tag{18}$$

$$\sigma_{ij}^{p(0)} = (1 + \frac{\varepsilon}{1+i\omega}e^{i\omega t})\bar{\sigma}_{ij}^{p(0)} \tag{19}$$

$$= (1 + \frac{\varepsilon}{1+i\omega}e^{i\omega t})(2\bar{E}_{ij}^{(0)}) \tag{20}$$

Eq. (20) indicates linear viscoelastic response even if $\mathrm{De} \to 0$, which is to say, if $\lambda\Omega \ll 1$ but ω (made dimensionless by λ) $\sim \mathcal{O}(1)$. On the other hand, if ω is also negligible, Eq. (20) reduces to $1 + \varepsilon e^{i\omega t}(2E_{ij}^{(0)})$, i.e. Newtonian flow.

The Stokes equation at zero-th order is hence:

$$\nabla_i p^{(0)} = \beta(1 + \varepsilon e^{i\omega t})\nabla^2\bar{u}_i^{(0)} + (1-\beta)(1 + \frac{\varepsilon}{1+i\omega}e^{i\omega t})\nabla^2\bar{u}_i^{(0)} \tag{21}$$

Using the ansatz that the pressure is the product of a temporal coefficient and the spacial component $\bar{p}^{(0)}$, and identifying the corresponding form for each with Eq. (21):

$$p^{(0)} = \left[1 + \varepsilon(\beta + \frac{1-\beta}{1+i\omega}e^{i\omega t})\right]\bar{p}^{(0)} \tag{22}$$

$$\nabla_i\bar{p}^{(0)} = \nabla^2\bar{u}_i^{(0)} \tag{23}$$

This shows the spatial components of the zero-th order pressure and velocity correspond to the Newtonian Stokes solutions. Due to the reversibility of Stokes flow, no propulsion is created at this order. Further, because the Newtonian problem is for an axisymmetric swirling body rotating in a Newtonian quiescent fluid, no pressure is generated and $p^{(0)}$ is identically zero [25].

$$p^{(0)} = 0 \tag{24}$$

As a consequence, the time-dependence of the velocity and polymer stress are not coupled by the pressure at zero-th order and $\bar{u}_i^{(0)}$ is a harmonic function. Eqs. (18), (20) and (24) are the general solutions for an axisymmetric swirler in an unbounded viscoelastic fluid at zero order in De.

2.2.2. $\mathcal{O}$ (De) solution for pressure, velocity and polymer stress

At linear order in the perturbation expansion, the governing equations are as follows:

$$0 = -\nabla_i p^{(1)} + \beta\nabla^2 u_i^{(1)} + (1-\beta)\nabla_j \sigma_{ij}^{p(1)} \tag{25}$$

$$\nabla_i u_i^{(1)} = 0 \tag{26}$$

$$\frac{\partial \sigma_{ij}^{p(1)}}{\partial t} + \sigma_{ij}^{p(1)} = M_{ij} - \alpha\sigma_{ik}^{p(0)}\sigma_{kj}^{p(0)} + 2E_{ij}^{(1)} \tag{27}$$

$$M_{ij} = -u_k^{(0)}\nabla_k \sigma_{ij}^{p(0)} + \nabla_k u_i^{(0)}\sigma_{jk}^{p(0)} + \nabla_k u_j^{(0)}\sigma_{ik}^{p(0)} \tag{28}$$

As before, we assume the linear-order pressure, velocity and polymer stress fields are the product of spatial and temporal dependent functions. Given the time-dependence of the imposed oscillation, we use an ansatz for the functional form of the linear-order pressure and velocity, where f and g are complex numbers to be determined from the governing equations at this order. Substituting for the linear-order polymer stress:

$$u_i^{(1)} = \bar{u}_i^{(1)} + f e^{i\omega t}\bar{u}_i^{(1)};\ E_{ij}^{(1)} = \bar{E}_{ij}^{(1)} + f e^{i\omega t}\bar{E}_{ij}^{(1)} \tag{29}$$

$$p^{(1)} = \bar{p}^{(1)} + g e^{i\omega t}\bar{p}^{(1)} \tag{30}$$

$$\sigma_{ij}^{p(1)} = \bar{M}_{ij} - \alpha\bar{\sigma}_{ik}^{p(0)}\bar{\sigma}_{kj}^{p(0)} + 2\bar{E}_{ij}^{(1)} \tag{31}$$

$$+ e^{i\omega t}\left[\frac{\varepsilon(2+i\omega)}{(1+i\omega)^2}\bar{M}_{ij} - \frac{2\varepsilon\alpha}{(1+i\omega)^2}\bar{\sigma}_{ik}^{p(0)}\bar{\sigma}_{kj}^{p(0)} + \frac{2f}{1+i\omega}\bar{E}_{ij}^{(1)}\right] + \mathcal{O}(\varepsilon^2) \tag{32}$$

$$\bar{M}_{ij} = -\bar{u}_k^{(0)}\nabla_k\bar{\sigma}_{ij}^{p(0)} + \nabla_k\bar{u}_i^{(0)}\bar{\sigma}_{jk}^{p(0)} + \nabla_k\bar{u}_j^{(0)}\bar{\sigma}_{ik}^{p(0)} \tag{33}$$

At this point, we discard terms quadratic in ε from Eq. (32) assuming $\varepsilon \ll 1$. We note that at $\mathcal{O}(\mathrm{De}^0)$, there are no terms of higher power than $\mathcal{O}(\varepsilon^1)$ for $\epsilon \ll 1$. Thus, our expansion to this point is truncated at terms linear in De, ε, and εDe. Substituting this into Eq. (25) and isolating the steady terms as well as the terms that vary as $e^{i\omega t}$:

$$\nabla_i\bar{p}^{(1)} = \nabla^2\bar{u}_i^{(1)} + (1-\beta)\nabla_j\bar{M}_{ij} - (1-\beta)\alpha\nabla_j\bar{\sigma}_{ik}^{p(0)}\bar{\sigma}_{kj}^{p(0)} \tag{34}$$

$$g\nabla_i\bar{p}^{(1)} = f\left(\frac{1+i\beta\omega}{1+i\omega}\right)\nabla^2\bar{u}_i^{(1)} + (1-\beta)\frac{\varepsilon(2+i\omega)}{(1+i\omega)^2}\nabla_j\bar{M}_{ij} \tag{35}$$

$$- (1-\beta)\frac{2\varepsilon\alpha}{(1+i\omega)^2}\nabla_j\bar{\sigma}_{ik}^{p(0)}\bar{\sigma}_{kj}^{p(0)} \tag{36}$$

As explicitly shown in the Appendix, Eq. (B.9) can be used to simplify $\nabla_j\bar{M}_{ij}$:

$$\nabla_j\bar{M}_{ij} = -\nabla_i\left(\bar{u}_j^{(0)}\nabla_j\bar{p}^{(0)} + \bar{E}_{jk}^{(0)}\bar{E}_{jk}^{(0)}\right) + \nabla_j\bar{\sigma}_{ik}^{p(0)}\bar{\sigma}_{kj}^{p(0)} \tag{37}$$

Since $\bar{p}^{(0)} = 0$:

$$\nabla_i(\bar{p}^{(1)} + (1-\beta)\bar{E}_{jk}^{(0)}\bar{E}_{jk}^{(0)}) = \nabla^2\bar{u}_i^{(1)} + (1-\beta)(1-\alpha)\nabla_j\bar{\sigma}_{ik}^{p(0)}\bar{\sigma}_{kj}^{p(0)} \tag{38}$$

$$g\nabla_i(\bar{p}^{(1)} + (1-\beta)\bar{E}_{jk}^{(0)}\bar{E}_{jk}^{(0)}) = f\left(\frac{1+i\beta\omega}{1+i\omega}\right)\nabla^2\bar{u}_i^{(1)} \tag{39}$$

$$+ (1-\beta)\frac{\varepsilon(2-2\alpha+i\omega)}{(1+i\omega)^2}\nabla_j\bar{\sigma}_{ik}^{p(0)}\bar{\sigma}_{kj}^{p(0)} \tag{40}$$

In order to satisfy Eq. (25) for all time, the ratio of the temporal coefficients of each term between Eqs. (38) and (40) must be equal. This leads to the following relations for the unknowns f, g:

$$g = \frac{\varepsilon(2-2\alpha+i\omega)}{(1+i\omega)^2(1-\alpha)} \tag{41}$$

$$f = \frac{\varepsilon(2-2\alpha+i\omega)}{(1+i\omega)(1+i\beta\omega)(1-\alpha)} \tag{42}$$

2.3. Head rotation of a freely-suspended swirler

The previous sections derive the $\mathcal{O}(\mathrm{De}^0)$ and $\mathcal{O}(\mathrm{De}^1)$ fields for a swirling axisymmetric body with a time-dependent rate of rotation — however, the body was not torque-free. The freely-suspended swimmer is comprised of two counter-rotating bodies, and the rotation rate of the head is such that the torque on the head is equal to that on the tail. In Appendix A, we show that the torque on the head has an $\mathcal{O}(\mathrm{De}^0)$ contribution and no $\mathcal{O}(\mathrm{De}^1)$ contribution, from perturbation in De. As a consequence, the head always rotates with the same time-dependence as the tail, but in the opposite direction. Hence, no additional time-dependence in the boundary conditions is introduced by including a counter-rotating head, and a single specified time-dependence is applicable for both the head and the tail velocity boundary conditions through $\mathcal{O}(\mathrm{De}^1)$. This applies for arbitrary axisymmetric geometries of the head and tail.

2.4. Translational velocity of a freely-suspended swirler

The analysis in the preceding sections has been derived for the unsteady velocity field created by a freely-suspended swirler with time-dependent rotation rate $\Omega(t) = 1 + \varepsilon e^{i\omega t}$. However, the experimentally measured quantity is typically the *translational velocity* of this swirler [12,14]. To relate these quantities, we use the reciprocal theorem. We quote the general form of the reciprocal theorem in viscoelastic fluids, with extended derivations found in previous work, e.g. [11]

$$\sum_{H,T}\left[\bar{U}_i F_i^{\mathrm{aux}} + \Omega_i L_i^{\mathrm{aux}} - U_i^{\mathrm{aux}} F_i - \Omega_i^{\mathrm{aux}} L_i\right] = \mathrm{De}\,(1-\beta)\int_V (\nabla_j u_i^{\mathrm{aux}})(\bar{M}_{ij} - \alpha\bar{\sigma}_{ik}^{p(0)}\bar{\sigma}_{kj}^{p(0)})\,dV \tag{43}$$

We consider the auxiliary problem of the same axisymmetric object, translating steadily with velocity U_i^{aux} along its axis of symmetry in a Newtonian fluid with non-dimensional viscosity $\beta^{\mathrm{aux}} = 1$; the auxiliary rotation rate and torque are hence both identically zero. We also consider the primary problem where the swimmer is force-free. Finally, we apply the identity derived in the Appendix (Eq. (B.20)) appropriate for rigid swirling motion to simplify the integral.

$$\bar{U}_i F_i^{\mathrm{aux}} = \mathrm{De}\,(1-\beta)\int_V (\nabla_j u_i^{\mathrm{aux}})\bar{\sigma}_{ik}^{p(0)}\bar{\sigma}_{kj}^{p(0)}\,dV \tag{44}$$

Since the auxiliary force is arbitrary, this equation gives the translational velocity of the freely-suspended swirler with a steadily-rotating tail as:

$$\bar{U}_i = \mathrm{De}\,(1-\beta)(1-\alpha)V^*\delta_{i3} \tag{45}$$

$$V^* = -\frac{1}{|F^{\mathrm{aux}}|}\int_V (\nabla_j u_i^{\mathrm{aux}})\bar{\sigma}_{ik}^{p(0)}\bar{\sigma}_{kj}^{p(0)}\,dV \tag{46}$$

The factor V^* accounts for the effect of the geometry of the swirler, and the magnitude and direction of its translation independently of the material properties of the fluid. A negative value indicates the swimmer is translating in the same direction as the swimmer in the auxiliary problem, and vice versa. This approach is similar to that appearing in previous work for the velocity of steadily-rotating swirlers [11]. In the present work, we derive a further result which shows linearity of $\bar{U}_i$ in α, and combine this with the unsteady perturbation results in Section 2.2 to get both the magnitude and time-dependence of the unsteady swimmer translational velocity in Section 2.4.1.

The integral in V^* can be computed by solving two Newtonian Stokes problems. In the first problem, we simulate the same swimmer translating along its axis of symmetry in a Newtonian fluid of the same zero-shear viscosity as the viscoelastic fluid of interest. Solving for the flow field around, and net force on, the swimmer. we get u_i^{aux} and F_i^{aux} respectively. On the other hand, as described in Section 2.2.1, $\bar{E}_{ij}^{(0)}$ can be obtained from the flow created by the swimmer rotating (torque-free) in a Newtonian fluid. Hence, the steady swim velocity of a freely-suspended swirler in a viscoelastic fluid can be computed from solving two Newtonian problems, without completing computer simulations in a viscoelastic fluid. This can be used as a method for quickly iterating through axisymmetric swirler geometries, in order to predict geometries that exhibit greater propulsion for better experimental measurements.

2.4.1. Tail rotation rate follows oscillation about a mean rotation rate

To obtain the transient velocity of the freely-suspended swirler, we note that the swirler's translational velocity is created by the linear-order velocity field, which is a product of a temporal coefficient and the steady field $\bar{u}_i^{(1)}$. The swirler translational velocity is thus also composed of a magnitude determined by the steady field – Eq. (45) – multiplied by a temporal coefficient. The temporal coefficient of the linear-order velocity field is the same throughout the fluid domain, including on the swirler surface; it is thus the same temporal coefficient derived in Section 2.2.2. thus for tail rotation rate $\Omega(t) = 1 + e^{i\omega t}$, the swirler has velocity:

$$U_i^{\text{trans}}(t) = \left(1 + \frac{\epsilon(2 - 2\alpha + i\omega)}{(1 + i\omega)(1 + i\beta\omega)(1 - \alpha)} e^{i\omega t}\right)\bar{U}_i \tag{47}$$

This result shows the translational velocity oscillates about an offset, with a phase shift compared to the oscillation of the rotating tail. The phase shift, or equivalently the in- and out-of-phase (with respect to the tail oscillation) amplitudes of the oscillating velocity are affected by fluid properties and hence a measurement of the fluid rheology. The experimentally-measured value of interest are the phase amplitudes of the translational velocity about its mean value, which we will refer to as the complex velocity U^*, analogous to the complex viscosity or complex modulus:

$$U^* = \frac{\epsilon(2 - 2\alpha + i\omega)}{(1 + i\omega)(1 + i\beta\omega)(1 - \alpha)} \tag{48}$$

We show in Section 3 how this functional form of the complex velocity compares to simulation results, and how this can be used to recover fluid parameters such as β, λ, α from simulation results.

Finally, we note that the above derivation does not require that the swirler be torque-free, only that it is force-free. Hence, the predictions for steady and transient velocity can also be extended to swirlers propelled by means of an externally-applied torque [12].

2.4.2. Tail rotation rate follows step-start or step-stop

The translational velocity of a freely-suspended swirler including a tail rotation rate following a step-start or step-stop – $\Omega_T(t) = \theta(t)$ and $\Omega_T(t) = 1 - \theta(t)$ respectively, where $\theta(t)$ is the Heaviside step function – can also be easily analyzed. This is analogous to start-up and cessation of stress tests in a benchtop rheometer. We have derived a general expression for the temporal coefficients via convolutions, as detailed in Appendix C, and apply it to this problem. For a single-mode Giesekus fluid, the translational velocity for a freely-suspended swirler is given through $\mathcal{O}(\text{De}^1)$ as follows:

$$\Omega_T(t) = \theta(t) : \frac{U(t)}{\bar{U}} = 1 + \frac{\beta(1 - 2(1 - \alpha)\beta e^{-t/\beta})}{(1 - \alpha)(1 - \beta)(1 - 2\beta)} \tag{49}$$

$$- \frac{\alpha e^{-2t}}{(1 - \alpha)(1 - \beta)} - \frac{(1 - 2\alpha)e^{-t}}{(1 - \alpha)(1 - \beta)} \tag{50}$$

$$\Omega_T(t) = 1 - \theta(t) : \frac{U(t)}{\bar{U}} = \frac{1}{1 - \alpha} e^{-t/\beta} - \frac{\alpha e^{-2t}}{(1 - \alpha)(1 - 2\beta)} \tag{51}$$

For an Oldroyd-B fluid where $\alpha = 0$:

$$\Omega_T(t) = \theta(t) : \frac{U(t)}{\bar{U}} = 1 + \frac{\beta e^{-t/\beta} - e^{-t}}{1 - \beta} \tag{52}$$

$$\Omega_T(t) = 1 - \theta(t) : \frac{U(t)}{\bar{U}} = e^{-t/\beta} \tag{53}$$

We show in Section 3 how the functional forms in Eqs. (52) and (53) compare to simulation results.

2.5. Numerical calculations

Three dimensional simulations of the governing equations and boundary conditions were performed using a third-order-accurate finite-volume flow solver developed at Stanford's Center for Turbulence Research. The numerical calculations for these problems closely follow the framework described in previous studies [14,15]. In brief, an unstructured, tetrahedral, body-fitted mesh (Fig. 2(b)) is used to define the fluid domain: the fluid region interior to a cylindrical boundary and exterior to the swimmer centered within this cylinder. The swimmer is always axisymmetric, with its axis of revolution aligned to that of the cylindrical boundary. The cylindrical domain has length and diameter 20 R_L, such that confinement effects are negligible. The co-moving frame of reference is adopted in this problem to avoid the need for remeshing and swimmer position updates. The mesh has increasing resolution around the swimmer at the center of the domain, in order to resolve any stress boundary layers there (Fig. 2(b)). The evolution equations for the velocity and polymer conformation tensor (Eq. (3), (7)) are solved on this mesh using the log-conformation method [26, 27] to maintain positive-definiteness. The initial conditions for the simulations are a quiescent fluid containing polymers at equilibrium, i.e. $\sigma_{ij}^p(t = 0) = 0$ everywhere. The boundary conditions for the conformation tensor are $\sigma_{ij}^p = 0$ at the entrance to the domain, and a convective outlet boundary at the exit. The tail of the swimmer has a rotation rate which can be prescribed as a function of time. At each timestep, inner iterations via a quasi-Newton method, specifically Broyden's method [28], are used to determine the swimmer's translational velocity, and the rotation rate of its head, such that the net force and torque on the swimmer are both zero.

The phase amplitudes of the translational velocity are analyzed to compare against theoretical predictions, as depicted in Fig. 2(c): the simulation is run for sufficient time such that the results are independent of the initial condition (after about 8λ). The last full oscillation period of the tail rotation rate is used for analysis: the in- and out-of-phase translational velocity phase amplitudes are calculated by numerical integration of the inner product with, respectively, the cosine and sine of the imposed frequency. The in-, and out-of-phase amplitudes respectively correspond to the real, and negative imaginary, components of the oscillation coefficient in Eq. (48)

For the results presented, the geometry of the swirler is kept the same unless otherwise indicated: a two-sphere swirler with a tail of radius $R_T = R_H/2$, separated by a gap of height $h = 0.05\, R_H$; Fig. 2(a) depicts this geometry to scale. The swirler is freely-suspended unless otherwise stated.

3. Results and discussion

3.1. Single-mode Oldroyd-B fluid

3.1.1. Reciprocal theorem

As described in Section 2.4, the translational velocity of a freely-suspended two-sphere swirler was predicted by running two Newtonian simulations and calculating the integral defined in Eq. (46) to obtain the geometric factor V^*. This factor was then scaled by the viscoelastic fluid properties De and β to predict the swirler's translational velocity. Fig. 3(a) shows these predictions for a range of De at three different values of β, compared to fully-resolved numerical simulations at the same conditions, for a swirler with a spherical head and tail as described in Section 2.5. Eq. (45) gives a prediction that translational velocity is linear in $(1-\beta)$, so normalizing the translational velocity by $(1-\beta)$ and with $\alpha = 0$, the results should collapse onto a single curve. Fig. 3(b) shows this procedure applied to the data from Fig. 3(a), and that the data indeed collapses onto a single curve at low De, with the slope calculated from Eq. (46). Additionally, we run steady simulations of a swirler with a different geometry: an oblate spheroidal tail with major radius 0.75 and minor radius 0.5, and a gap size $h = 0.15$. Using the same procedure to calculate V^* and comparing this prediction to simulation results, we again see our results show good agreement with the theory for De ≤ 1, indicating that the steady swim velocity for a freely-suspended

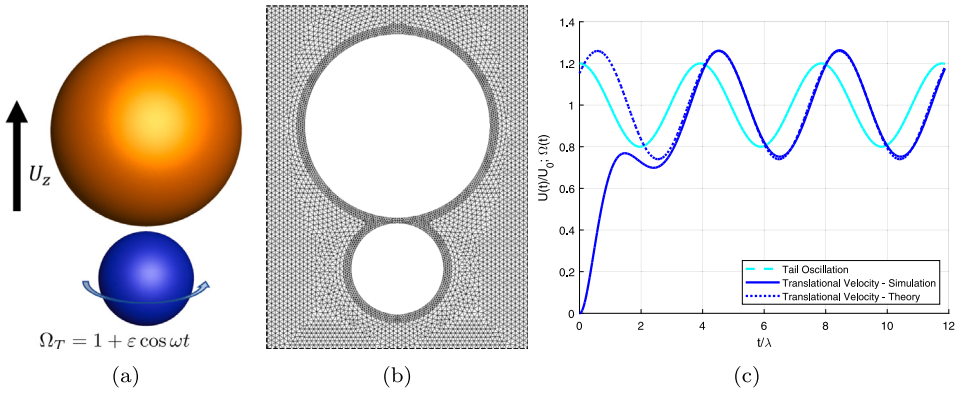

Fig. 2. Simulation setup and analysis: (a) representative geometry with time-dependent tail rotation, here shown as oscillation about a constant offset; (b) meshing of the body-fitted simulation domain with refined mesh layers near the swimmer body; and (c) representative translational velocity extracted from simulation and compared to theoretical predictions.

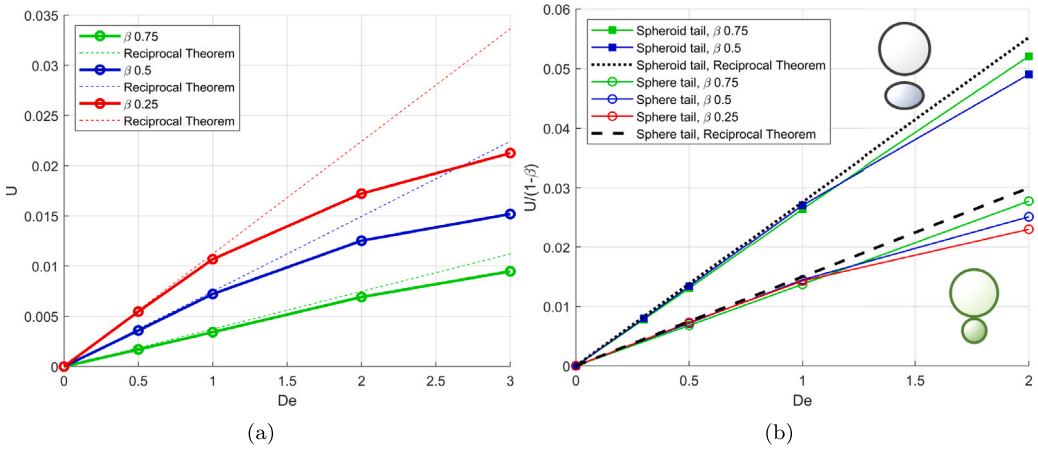

Fig. 3. Using the reciprocal theorem to predict the translational velocity of a freely-suspended swirler. In these plots, the points are from steady simulations of freely-suspended swirlers in single-mode Oldroyd-B fluids with varying parameters De and β. The slopes of the dashed lines and dotted lines are obtained from calculating V^* (Eq. (46)) from Newtonian simulations. (a) Swirler translational velocity plotted against De, for three different β values. The swirler has a spherical head and spherical tail, as described in Section 2.5. (b) Swirler translational velocity normalized by $(1-\beta)$, for two different geometries. The data from Fig. 3a collapses onto a single curve in agreement with theory. The data for a swirler with an oblate spheroid tail also collapses, and has a higher translational velocity under the same material parameters. The insets show representative sketches of the two swirler geometries.

swirler can be predicted from the results of two Newtonian simulations, the latter of which are less computationally intensive to complete than fully-resolved viscoelastic simulations. Further, this procedure can be applied to arbitrary axisymmetric geometries, serving as a design tool to allow for faster iteration through multiple swirler design geometries to find those, for example, with enhanced propulsion.

3.1.2. Step-start and step-stop

Fig. 4 shows predictions for the translational velocity when the swirler is immersed in a single-mode Oldroyd-B fluid, with a step change in its tail rotation. Predictions from the theoretical results obtained in Section 3.1.2, Eqs. (52) and (53), are shown in Figs. 4(a) and 4(b) respectively. There is good agreement between our theoretical predictions and simulation results, indicating our theory captures the transient physics accurately, again for De ≤ 1. In particular, Eq. (53) indicates the timescale of the decay in the translational velocity in dimensional terms is $\beta\lambda$, i.e. the so-called retardation time, and so fitting this decay can be used as another measure of these parameters.

3.1.3. Oscillation

Fig. 5 shows predictions for the complex translational velocity when the swirler is immersed in a single-mode Oldroyd-B fluid, with its tail having a rotation rate that oscillates with time about a constant mean. The amplitude of this oscillation is small compared to the magnitude of the mean — here, the oscillation amplitude is 20% of the mean oscillation rate. The complex velocity is a function of the non-dimensional Oldroyd-B parameter β and the oscillation frequency non-dimensionalized by λ. Fig. 5a shows the effect of different β on the complex velocity, changing the intersection of the in- and out-of-phase amplitudes, and the maximum of the out-of-phase amplitude. The curves are plotted from the expressions derived in Section 2, and the points are results obtained from simulations in a fluid where the mean Deborah number is 0.3. There is good agreement between our theoretical predictions and simulation results at different values of β, indicating our theory captures the transient physics accurately.

We further wish to understand the range of the mean Deborah number for which our perturbation theory expressions are valid. To that end, we conduct simulations at a constant value of β but with three different De values — this is equivalent to having the swirler rotate with the same mean tail rotation rate and oscillation frequencies, but in single-mode fluids of different relaxation times. Fig. 5b shows the results of these simulations plotted as points, compared to theoretical predictions (Eq. (48)) with $\beta = 0.75$. We see the results obtained at different mean Deborah numbers collapse onto the same curve, indicating the perturbation theory is robust up to at least $De = 0.8$.

Finally, we observe that the non-dimensional complex viscosity for a Maxwell mode can be recovered from the complex velocity U^* as defined in Eq. (48) using the following relation:

$$\frac{\eta_M^*}{\eta_p} = \frac{1}{1+i\omega} \tag{54}$$

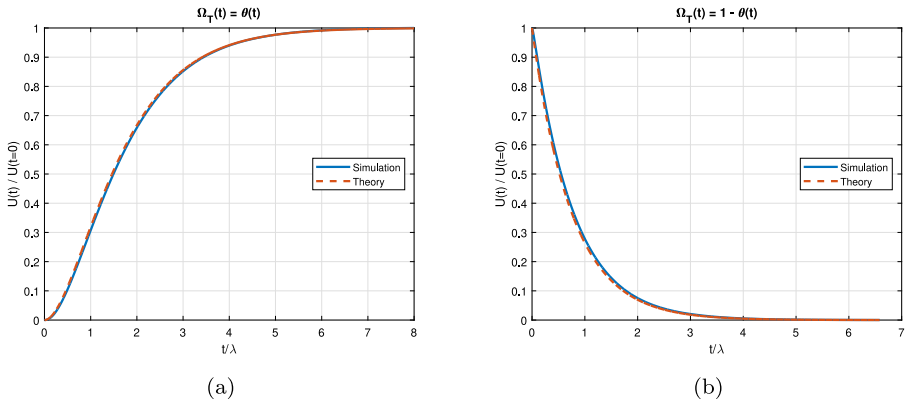

Fig. 4. Translational velocity of a swirler with step change in tail rotation in a single-mode Oldroyd-B fluid, De = 0.3, $\beta = 0.75$. (a) Swirler tail rotation rate undergoes a step change to its steady value. (b) Swirler tail rotation rate undergoes a step change from a steady value to zero.

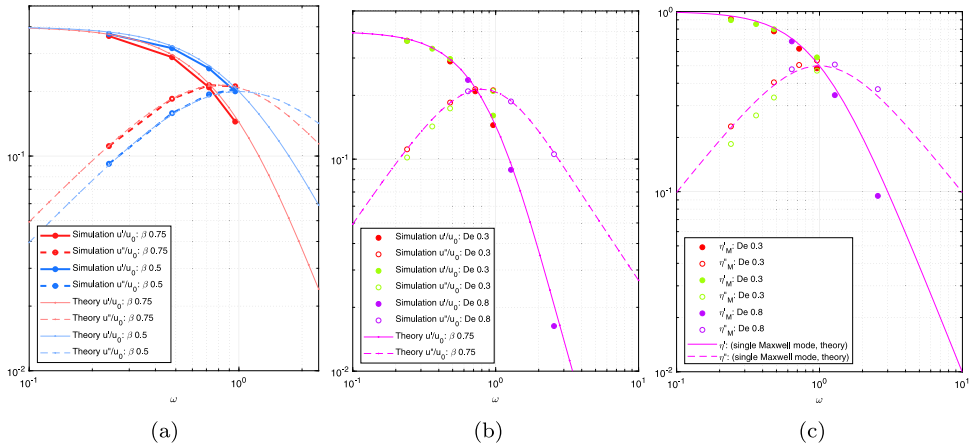

Fig. 5. Translational velocity of a swirler with oscillating tail rotation in a single-mode Oldroyd-B fluid, investigating (a) the in- and out-of-phase swirler translational velocities at different values of β and constant mean Deborah number of 0.3; (b) the in- and out-of-phase swirler translational velocities at different mean Deborah numbers and constant $\beta = 0.75$; and (c) converting the complex velocity into the dimensionless complex viscosity for the Maxwell mode in the Oldroyd-B fluid.

$$= U^*\left(\frac{1+i\beta\omega}{\epsilon}\right) - 1 \tag{55}$$

Hence the nondimensional complex viscosity can be recovered using measurements from an experiment or simulation as follows:

$$\frac{\eta_M^*}{\eta_p} \approx U^*_{\text{measured}}\left(\frac{1+i\beta\omega}{\epsilon}\right) - 1 \tag{56}$$

$$U^*_{\text{measured}} \equiv U'_{\text{measured}} - iU''_{\text{measured}} \tag{57}$$

In (57), $U'_{\text{measured}}, U''_{\text{measured}}$ are respectively the in- and out-of-phase velocity amplitudes recovered from the translational velocity from an experiment or simulation, and ϵ is known from the imposed tail oscillation rate. In Fig. 5(c) we perform this transformation on the complex velocity and see good agreement with the theoretical prediction for the corresponding Maxwell mode in the Oldroyd-B fluid.

3.2. Single-mode Giesekus fluid

We also investigate the complex velocity, scaled to the mean velocity, produced by a swirler immersed in a single-mode Giesekus fluid. We first test the prediction that the steady velocity is linear in $(1-\alpha)$, where α is the Giesekus parameter and leads to both shear-thinning and non-zero second normal stresses [21]. The points in Fig. 6(a) shows simulation results for the translational velocity of a swirler whose tail has a constant rotation rate, normalized by the velocity when $\alpha = 0$. The deviation of the simulation results from the expected scaling increases as α increases but is still accurate to within 4%. Our analytical theory is hence able to capture the scaling of the steady velocity with α observed in simulations.

For a tail rotation rate with oscillations, Fig. 6b-d shows theoretical predictions of the effect of the Giesekus parameter α on the complex viscosity, for a swirler in a single-mode Giesekus fluid. As with the Oldroyd-B fluid, β also shifts the phase amplitude curves, their intersection and maxima.

Fig. 6(e) compares the results, both from simulation (points) and theory (lines), between a Giesekus fluid (data in blue) with $\alpha = 0.1$ and an Oldroyd-B fluid (i.e. a Giesekus fluid with $\alpha = 0$; data in red). The value of β is maintained at 0.75 for both cases. For each simulation, the complex velocity scaled to the mean velocity is plotted. There is good agreement between the simulation results and theoretical predictions, demonstrating how non-zero second normal stresses modestly affect the translational velocity, and that our model captures the steady and transient physics for fluids with non-zero second normal stresses.

We also note that the $\mathcal{O}(\text{De}^1)$ expansion of the Giesekus fluid corresponds to the second-order fluid model, with the constants transformed as per Table 6.2-2 in Ref. [21]: λ_1, λ_2 in the reference correspond to λ and $(1-\beta)\lambda$ in this text respectively.

3.3. Multi-mode Oldroyd-B fluid

Most real polymeric fluids contain a spectrum of relaxation times [29]. We extend our formula for the complex velocity to multi-mode Oldroyd-B fluids, detailed in Appendix D, and run simulations of our swirler in these fluids to compare against the theoretical predictions.

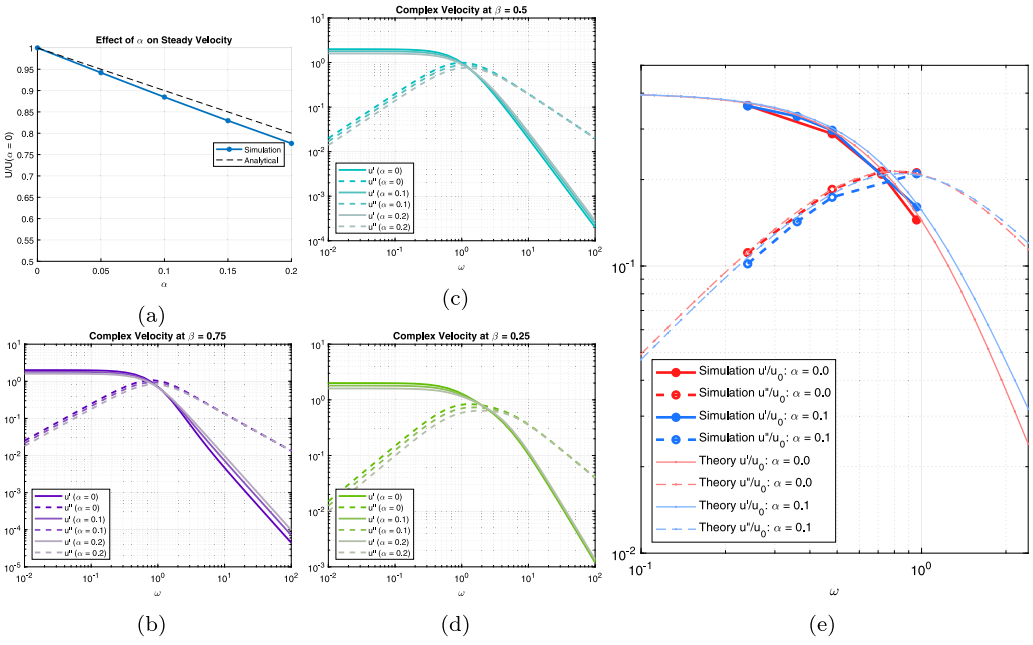

Fig. 6. Complex velocity of a swirler with oscillating tail rotation in a single-mode Giesekus fluid, investigating (a) the effect of the Giesekus mobility parameter α on the translational velocity of a swirler with steady tail rotation; (b-d) theoretical predictions of the in- and out-of-phase swirler translational velocities at different values of (α, β); and (e) simulation results against theoretical predictions at two values of α for constant $\beta = 0.75$, De $= 0.3$.

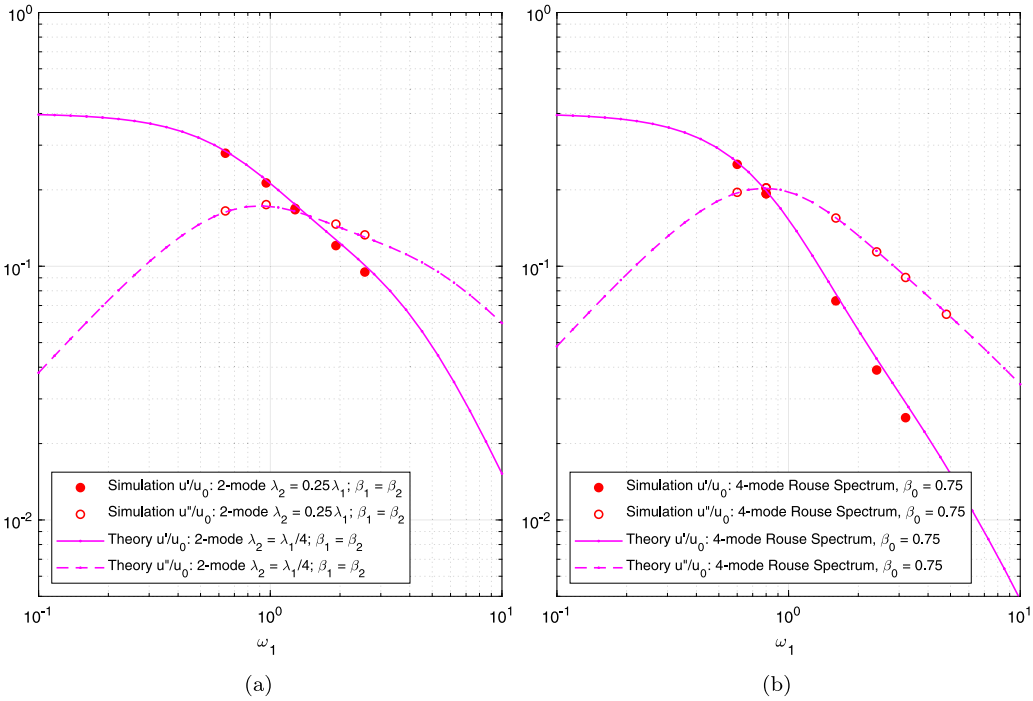

Fig. 7. Complex velocity of a swirler with oscillating tail rotation in a multi-mode Oldroyd-B fluid. In each plot, the oscillation frequency is non-dimensionalized by the longest relaxation time. (a) Two-mode Oldroyd-B fluid with $\beta = 0.5$; and (b) 4-mode Oldroyd-B fluid where the modes follow the Rouse relaxation spectrum, $\beta = 0.75$.

For these frequency sweeps, reported in Fig. 7, the oscillation frequency ω_1 is made dimensionless by the longest relaxation time.

We first use a two-mode Oldroyd-B fluid as a test case. Fig. 7(a) shows the results from a frequency sweep in such a fluid, compared to predictions from theory. We again see good agreement for this simple test case.

For more accurate representation of experimental polymeric fluids, we look at well-known models for polymer solutions – e.g. the Rouse or Zimm models – which predict a spectrum of relaxation times for polymeric fluids. In these spectrums, the relaxation times and polymer viscosities typically scale according to the mode number. For instance, the Rouse model predicts a spectrum where the first mode has the longest relaxation time λ_1 and highest polymer viscosity $\eta_{p,1}$, and subsequent modes have relaxation times and polymer viscosities scale as the inverse square of the mode number: $\lambda_q = \lambda_1/q^2$; $\eta_{p,q} = \eta_{p,1}/q^2$, where q is the mode number. Equivalently, this indicates that the ratio between the relaxation time and polymer frequency for each mode is a constant. We run a frequency sweep in a multi-mode Oldroyd-B fluid

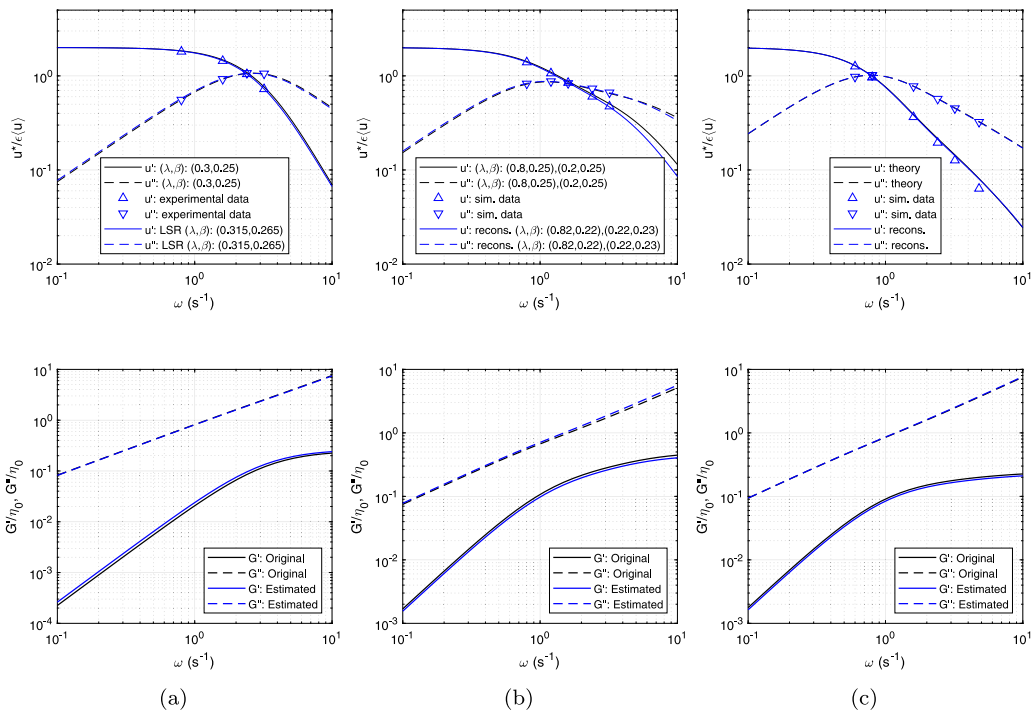

Fig. 8. Fitting simulation results (top plots) to functional forms from theory via least squares regression to reconstruct dimensionless complex modulus (bottom plots) for a (a) single-mode, (b) two-mode, and (c) four-mode Oldroyd-B relaxation spectrum. In the first two cases, the viscosity and relaxation time of each mode is treated as a fitting parameter; in the final case, the number of modes is specified, and the relaxation time of each mode, plus a constant scale factor that linearly relates viscosity and relaxation time, is treated as a fitting parameter.

with four modes employing the Rouse scaling for relaxation times and polymer viscosities. Fig. 7(b) shows the simulation results, compared to predictions from theory. The agreement between simulation and theory for both frequency sweeps indicates that our model captures the effect of having more than one relaxation modes, each with a distinct relaxation time and elastic modulus.

Due to the algebraic form of the multi-mode complex velocity, there is no straightforward algebraic transformation to recover the dimensionless complex viscosity as was done in Section 3.1.3. Instead, we investigate the use of least-squares regression to Eq. (D.19) to estimate the polymer relaxation spectrum, i.e. determine a list of modes with associated relaxation times and polymer viscosities. We test this procedure against simulation results collected for a frequency sweep in a 1-mode, 2-mode, and 4-mode Rouse fluid. In this section, we work in dimensional quantities to reflect a usual experimental procedure. The frequency tested in each simulation is hence reported in dimensional units (s^{-1}), and the polymer relaxation times are considered dimensionally as well. For the first two fluids, we let the mode relaxation times λ_q and polymer fractions β_q be free fitting parameters; this also fixes the solvent fraction $\beta = 1-\sum_q \beta_q$. For the Rouse fluid, we assume the relaxation time of each mode is a fitting parameter, with an additional fitting parameter being the ratio between the relaxation time and polymer viscosity common to all modes. Fig. 8 shows the results of using linear regression to simulation data to obtain the relaxation spectrum. We see good agreement between the relaxation time spectrum predicted from regression to the functional form of the complex velocity, and the actual relaxation time spectrum of the fluid used in each simulation. The relaxation time spectrum is then used to calculate the complex modulus modulo a constant factor of the zero-shear viscosity, via a sum of the multiple Maxwell modes:

$$\frac{G^*}{\eta_0} = i\omega\left(\beta + \sum_{q=1}^{n} \frac{\beta_q}{1+i\lambda_q\omega}\right) \tag{58}$$

We propose that this method can be used to analyze experimentally collected data from a physical swirler, to obtain the viscoelastic spectrum of the fluid in which it is immersed.

4. Conclusions

In this study, we have analyzed freely-suspended swirlers of arbitrary axisymmetric geometry in a viscoelastic fluid using analytical and numerical calculations to understand the interaction between unsteady swirling flows in viscoelastic fluids, and the unsteady propulsion generated by such flows. We show that the steady swim speed for an arbitrary axisymmetric geometry at low Deborah number can be calculated from the solution of two Newtonian problems in the same geometry, (Section 2.4). The latter calculation is far less computationally or mathematically intensive than solving the full viscoelastic problem. This formulation can thus be used as a design tool to search through the space of swirler geometry and optimize propulsion. The theory and numerical simulations predict a nearly linear increase in the speed with the Deborah number (i.e. fluid elasticity), $1-\beta$ (i.e. polymer concentration), and $1-\alpha$ (where α reflects the second normal stress coefficient) for $\mathrm{De} \leq 1$. Note that all of these parameters are of rheological interest. While we specifically consider the Giesekus model in this paper, the results can be expressed in terms of the second-order fluid model, where the Giesekus model parameters β and α can be re-expressed as first and second normal stress coefficients. This is appropriate for the low Deborah number limit, for which the perturbation expansion is also derived, and shows the linear proportionality of the translation speed in that regime; these predictions become less accurate as the Deborah number increases.

In addition to the steady swim speed, we investigate the unsteady swim speed produced by unsteady tail rotation. We derive a general form for the unsteady swim speed as a function of fluid material parameters and the unsteady tail rotation Appendix C, and for a specific form (oscillation about an offset). We then demonstrate how the functional

form of the unsteady swim speed is related to fluid material parameters (Section 2.4.1). These functional forms allow us to fit simulation data to reconstruct the viscoelastic spectrum of the suspending fluid, and from the spectrum make predictions of the fluid's linear viscoelastic response (Section 3.3). In general, the swirler translational velocity arises from a balance between the propulsion created by normal stresses proportional to the square of the tail rotation rate, and the drag exerted on the swirler as it translates through the fluid. For the tail rotation rate presented in Section 3.3, the propulsion lags the oscillating tail rotation rate, and the phase difference between the oscillating tail rotation and the oscillating propulsion increases with oscillation frequency. The propulsion magnitude also decreases with increasing oscillation frequency, as the normal stresses are unable to reach their steady values in each cycle of the tail oscillation rate. Since the swirler translates with an oscillating speed, there is also a phase difference between the drag and the speed: as with the unsteady translation of spheres through a viscoelastic fluid, the complex viscosity creates a phase difference. These effects together mean that at low oscillation frequencies, the propulsion is largely in-phase with the tail rotation rate and the in-phase velocity dominates, while at high oscillation frequencies the propulsion is largely out-of-phase with the tail rotation rate and diminishes in magnitude.

Together, the studies in this paper expand the design space of self-propelled swirlers [15] to allow the identification of geometries with increased propulsion for better signal-to-noise, and to perform different rheological tests by having different time-varying tail rotation rates. We note that the perturbation expansion of the Giesekus constitutive equation up to linear order in De has the same functional form as the general second order fluid model, where the model parameters are expressed as the primary and secondary normal stress coefficients. The results of these studies are thus broadly applicable to "weak" flows of complex fluids.

Declaration of competing interest

The authors declare the following financial interests/personal relationships which may be considered as potential competing interests: Boon Siong Neo reports financial support was provided by Agency for Science Technology and Research.

Data availability

Data will be made available on request.

Acknowledgments

This work was supported by the NSF Grant No. CBET 2210532. N. B. S. is supported by the Agency of Science Technology and Research, Singapore (A*STAR) NSS-PhD award. This work used the Anvil cluster at the Rosen Center for Advanced Computing, Purdue through allocation PHY220092 from the Advanced Cyberinfrastructure Coordination Ecosystem: Services & Support (ACCESS) program, which is supported by National Science Foundation, United States grants #2138259, #2138286, #2138307, #2137603, and #2138296.

Appendix A. Swimmer head rotation rate

Using the reciprocal theorem, we shall show that if the freely-suspended swirler has head and tail rotation rates that make the whole swirler torque free in a Newtonian fluid, the same rotation rates will let it be torque free in a weakly elastic fluid.

The surface of the head and tail are S_H, S_T respectively, and the total surface of the whole swirler is $S = S_H + S_T$. The primary problem is the force-free, but not necessarily torque-free, swirler in a weakly elastic fluid, i.e. the second order fluid expanded up to linear order in De, and with head and tail rotation rates Ω_i^H, Ω_i^T. The auxiliary problem is the swirler of the same geometry in a Newtonian fluid, *with the same head and tail rotation rates*: $\Omega_i^{H*} = \Omega_i^H, \Omega_i^{T*} = \Omega_i^T$. The (axisymmetric) swirler in the auxiliary problem is force-free as it only exhibits swirling motion.

Primary problem:

$$p = p^{(0)} + \mathrm{De}\, p^1 \tag{A.1}$$

$$u_i = u_i^{(0)} + \mathrm{De}\, u_i^1 \tag{A.2}$$

$$\sigma_{ij}^p = \sigma_{ij}^{p0} + \mathrm{De}\, \sigma_{ij}^{p(1)} \tag{A.3}$$

$$\sigma_{ij} = \sigma_{ij}^{(0)} + \sigma_{ij}^1 \tag{A.4}$$

$$= -p^{(0)}\delta_{ij} + 2E_{ij}^{(0)} + \mathrm{De}\left[-p^1\delta_{ij} + 2E_{ij}^1 + (1-\beta)\sigma_{ij}^{p(1)}\right] \tag{A.5}$$

$$= -p^{(0)}\delta_{ij} + 2E_{ij}^{(0)} \tag{A.6}$$

$$+ \mathrm{De}\left[-p^1\delta_{ij} + 2E_{ij}^1 + (1-\beta)\left(M_{ij} - 4\alpha E_{ik}^{(0)}E_{kj}^{(0)}\right)\right] \tag{A.7}$$

$$\nabla_j \sigma_{ij} = 0 \tag{A.8}$$

$$F_i^H + F_i^T = 0 \tag{A.9}$$

Auxiliary (Newtonian) problem:

$$\sigma_{ij}^* = -p^*\delta_{ij} + 2E_{ij}^* \tag{A.10}$$

$$\nabla_j \sigma_{ij}^* = 0 \tag{A.11}$$

$$F_i^{H*} + F_i^{T*} = 0 \tag{A.12}$$

Since the auxiliary and primary problems have the same boundary conditions on the pressure and velocity at $\mathcal{O}(\mathrm{De}^0)$, $p^* = p^{(0)}$ and $u_i^* = u_i^{(0)}$. We will use the equivalence between * and $^{(0)}$ quantities for simplification later. Constructing the reciprocal theorem:

$$\nabla_j(u_i\sigma_{ij}^* - u_i^*\sigma_{ij}) = u_i\cancelto{0}{\nabla_j\sigma_{ij}^*} - u_i^*\cancelto{0}{\nabla_j\sigma_{ij}} \tag{A.13}$$

$$+ (\nabla_j u_i)\sigma_{ij}^* - (\nabla_j u_i^*)\sigma_{ij} \tag{A.14}$$

$$-\int_S u_i\sigma_{ij}^* n_j - u_i^*\sigma_{ij}n_j\, dA = \int_V (\nabla_j u_i)\sigma_{ij}^* - (\nabla_j u_i^*)\sigma_{ij}\, dV \tag{A.15}$$

Simplifying the L.H.S.:

$$\int_S u_i\sigma_{ij}^* n_j\, dA = \Omega_j^H L_j^{H*} + \Omega_j^T L_j^{T*} + U_i\cancelto{0}{(F_i^{H*} + F_i^{T*})} \tag{A.16}$$

Similarly: $\int_S u_i^*\sigma_{ij}n_j\, dA = \Omega_j^{H*}L_j^H + \Omega_j^{T*}L_j^T + U_i^*\cancelto{0}{(F_i^H + F_i^T)}$ (A.17)

$$-\int_S u_i\sigma_{ij}^* n_j - u_i^*\sigma_{ij}n_j\, dA = -(\Omega_j^H L_j^{H*} + \Omega_j^T L_j^{T*}) - (\Omega_j^{H*}L_j^H + \Omega_j^{T*}L_j^T) \tag{A.18}$$

$$= -\Omega_j^H(L_j^{H*} - L_j^H) - \Omega_j^T(L_j^{T*} - L_j^T) \tag{A.19}$$

Simplifying the R.H.S.:

$$\int_V (\nabla_j u_i)\sigma_{ij}^*\, dV = \int_V (E_{ij}^{(0)} + \mathrm{De}\, E_{ij}^1)(2E_{ij}^*)\, dV \tag{A.20}$$

$$= \int_V 2E_{ij}^{(0)}E_{ij}^{(0)} + 2\mathrm{De}\, E_{ij}^1 E_{ij}^{(0)}\, dV \tag{A.21}$$

$$\int_V (\nabla_j u_i^*)\sigma_{ij}\, dV = \int_V E_{ij}^*(2E_{ij}^{(0)} + 2\mathrm{De}\, E_{ij}^1 + \mathrm{De}\,(1-\beta)\sigma_{ij}^{p(1)})\, dV \tag{A.22}$$

$$= \int_V 2E_{ij}^{(0)}E_{ij}^{(0)} + 2\mathrm{De}\, E_{ij}^1 E_{ij}^{(0)}\, dV \tag{A.23}$$

$$+ \int_V \mathrm{De}\,(1-\beta)\sigma_{ij}^{p(1)}E_{ij}^{(0)}\, dV \tag{A.24}$$

$$\int_V (\nabla_j u_i)\sigma_{ij}^* - (\nabla_j u_i^*)\sigma_{ij}\, dV = -\int_V \mathrm{De}\,(1-\beta)\sigma_{ij}^{p(1)}E_{ij}^{(0)}\, dV \tag{A.25}$$

$$= -\mathrm{De}\,(1-\beta)\int_V E_{ij}^{(0)}(M_{ij} - 4\alpha E_{ik}^{(0)}E_{kj}^{(0)})\, dV \tag{A.26}$$

Substituting Eqs. (A.19) and (A.26) to simplify the reciprocal theorem Eq. (A.15):

$$\Omega_j^H(L_j^{H*}-L_j^H)+\Omega_j^T(L_j^{T*}-L_j^T)=\mathrm{De}\,(1-\beta)\int_V E_{ij}^{(0)}(M_{ij}-4\alpha E_{ik}^{(0)}E_{kj}^{(0)})\,dV \tag{A.27}$$

As in Section 2.2.2, we use the Giesekus equation [21] to simplify the integral containing M_{ij}:

$$\int_V E_{ij}^{(0)}(M_{ij}-4\alpha E_{ik}^{(0)}E_{kj}^{(0)})\,dV=(1-\alpha)\int_V E_{ij}^{(0)}E_{ik}^{(0)}E_{kj}^{(0)}\,dV \tag{A.28}$$

$$\left[\Omega_j^H(L_j^{H*}-L_j^H)+\Omega_j^T(L_j^{T*}-L_j^T)\right]=\mathrm{De}\,(1-\beta)(1-\alpha)\int_V E_{ij}^{(0)}E_{ik}^{(0)}E_{kj}^{(0)}\,dV \tag{A.29}$$

The quantity $E_{ij}^{(0)}E_{ik}^{(0)}E_{kj}^{(0)}$ is the trace of the cube of the rate of strain tensor. Let the eigenvalues of E_{ij} be $\lambda_1,\lambda_2,\lambda_3$. Then:

$$E_{kk}^{(0)}=\lambda_1+\lambda_2+\lambda_3=0 \tag{A.30}$$

$$E_{ij}^{(0)}E_{ik}^{(0)}E_{kj}^{(0)}=\mathrm{tr}(E_{ik}^{(0)}E_{kl}^{(0)}E_{lj}^{(0)}) \tag{A.31}$$

$$=\lambda_1^3+\lambda_2^3+\lambda_3^3 \tag{A.32}$$

We observe that if at least one of $(\lambda_1,\lambda_2,\lambda_3)$ is zero, then the remaining eigenvalues have equal magnitude and opposite sign, meaning that the sum of their cubes is zero. We will now show that it is the case that at least one eigenvalue is zero.

A.1. Eigenvalues of the rate-of-strain tensor

We are interested in the eigenvalues of the rate-of-strain tensor for a flow created by an axisymmetric object rigidly rotating about its axis of revolution. Due to the axisymmetry of the problem, we identify that the flow can be expressed as derivatives of a streamfunction [30]. First, without loss of generality, we align the axis of rotation and revolution to the x_3 axis and note that the flow can be written in the following form:

$$u_i=\Omega\epsilon_{i3k}\nabla_k\phi \tag{A.33}$$

$$\nabla^2\phi(r_c,x_3)=0 \tag{A.34}$$

$$r_c=\sqrt{x_1^2+x_2^2} \tag{A.35}$$

$$E_{ij}=\frac{\Omega}{2}\left[\epsilon_{i3k}\nabla_j\nabla_k\phi+\epsilon_{j3k}\nabla_i\nabla_k\phi\right] \tag{A.36}$$

$$=\frac{\Omega}{2}\begin{bmatrix}-2\nabla_1\nabla_2\phi & \nabla_1^2\phi-\nabla_2^2\phi & -\nabla_2\nabla_3\phi\\ \nabla_1^2\phi-\nabla_2^2\phi & 2\nabla_1\nabla_2\phi & \nabla_1\nabla_3\phi\\ -\nabla_2\nabla_3\phi & \nabla_1\nabla_3\phi & 0\end{bmatrix} \tag{A.37}$$

Here, we work in cylindrical coordinates (r_c,θ_c,z_c) – with the subscript c to denote cylindrical coordinates – where the z_c axis is aligned to x_3 and correspondingly the axis of rotation and revolution. The Cartesian derivatives can then be rewritten in term of the cylindrical coordinates:

$$\nabla_1=\frac{x_1}{r_c}\frac{\partial}{\partial r_c}=\cos\theta_c\frac{\partial}{\partial r_c} \tag{A.38}$$

$$\nabla_2=\frac{x_2}{r_c}\frac{\partial}{\partial r_c}=\sin\theta_c\frac{\partial}{\partial r_c} \tag{A.39}$$

$$\nabla_1^2-\nabla_2^2=\left[\sin^2\theta_c-\cos^2\theta_c\right]\frac{\partial^2}{\partial r_c^2} \tag{A.40}$$

$$=\cos 2\theta_c\frac{\partial^2}{\partial r_c^2} \tag{A.41}$$

Using subscripts to denote derivatives where $(\cdot)_r=\frac{\partial}{\partial r_c}(\cdot)$, $(\cdot)_z=\frac{\partial}{\partial z_c}(\cdot)=\frac{\partial}{\partial x_3}(\cdot)$:

$$E_{ij}=\frac{\Omega}{2}\begin{bmatrix}-2\cos\theta_c\sin\theta_c\phi_{rr} & \cos 2\theta_c\phi_{rr} & -\sin\theta_c\phi_{rz}\\ \cos 2\theta_c\phi_{rr} & 2\cos\theta_c\sin\theta_c\phi_{rr} & \cos\theta_c\phi_{rz}\\ -\sin\theta_c\phi_{rz} & \cos\theta_c\phi_{rz} & 0\end{bmatrix} \tag{A.42}$$

$$\det(E_{ij})=-2\cos\theta_c\sin\theta_c\phi_{rr}(\sin\theta_c\phi_{rz})^2 \tag{A.43}$$

$$+2(\cos 2\theta_c\phi_{rr})(-\sin\theta_c\phi_{rz})(\cos\theta_c\phi_{rz}) \tag{A.44}$$

$$-(-2\cos\theta_c\sin\theta_c\phi_{rr})(\cos\theta_c\phi_{rz})^2 \tag{A.45}$$

$$=\phi_{cc}(\phi_{rz})^2\left[-\sin 2\theta_c\sin^2\theta_c-\cos 2\theta_c\sin 2\theta_c+\sin 2\theta_c\cos^2\theta_c\right] \tag{A.46}$$

$$=0 \tag{A.47}$$

This shows the determinant of the rate-of-strain tensor is zero, and thus at least one eigenvalue is zero. Hence, the trace of the cube of the rate-of-strain tensor is also zero. Returning to Eq. (A.29):

$$\Omega_j^H(L_j^{H*}-L_j^H)+\Omega_j^T(L_j^{T*}-L_j^T)=0 \tag{A.48}$$

We now use this result to determine the torques on the swirler head and tail, L_i^H and L_i^T, and show that they are the same as those in the Newtonian auxiliary problem, using proof by contradiction. If we assume the head and tail torques in the primary problem are different from those in the auxiliary problem, i.e. $L_i^H=L_i^{H*}+\Delta L_i^H$, $L_i^T=L_i^{T*}+\Delta L_i^T$:

$$\left[\Omega_j^H(\Delta L_j^H)+\Omega_j^T(\Delta L_j^T)\right]=0 \tag{A.49}$$

Since the head and tail counter-rotate, Ω_i^H and Ω_i^T are of different sign. The only non-zero solution to Eq. (A.49) requires ΔL_j^H and ΔL_j^T to be the same sign. However, this would cause the head and tail rotation to be offset in the same direction, and no other information can be used to determine the preferred direction. Hence we conclude that $\Delta L_j^H=\Delta L_j^T=0$ is the only physical solution.

This shows that if the head and tail rotation rates are the same in a weakly elastic fluid as they are for a Newtonian fluid, and the swirler is torque free in a Newtonian fluid, it will also be torque-free in the weakly elastic fluid. Crucially, the time-dependence of the head rotation rate will follow that of the tail, due to properties of the Newtonian Stokes regime. Thus only one time-dependence appears in the velocity boundary conditions, as used in Section 2.4.

Appendix B. Divergence of products of zero-th order terms

From a perturbation in De, the linear-order total stress is given by:

$$\bar{\sigma}_{ij}^{(1)}=-\bar{p}^{(1)}\delta_{ij}+2\beta\bar{E}_{ij}^{(1)}+\bar{\sigma}_{ij}^{p(1)} \tag{B.1}$$

$$\bar{\sigma}_{ij}^{p(1)}=(1-\beta)\left[2\bar{E}_{ij}^{(1)}-\bar{u}_k^{(0)}\nabla_k\bar{\sigma}_{ij}^{p(0)}+\nabla_k\bar{u}_i^{(0)}\bar{\sigma}_{jk}^{p(0)}+\nabla_k\bar{u}_j^{(0)}\bar{\sigma}_{ik}^{p(0)}\right] \tag{B.2}$$

$$=(1-\beta)\left[2\bar{E}_{ij}^{(1)}-2\left(\bar{u}_k^{(0)}\nabla_k\bar{E}_{ij}^{(0)}-\nabla_k\bar{u}_i^{(0)}\bar{E}_{jk}^{(0)}-\nabla_k\bar{u}_j^{(0)}\bar{E}_{ik}^{(0)}\right)\right] \tag{B.3}$$

For ease of convention we can rewrite the total stress in a cleaner form, collecting non-linear combinations of zeroth-order terms:

$$\bar{\sigma}_{ij}^{(1)}=-\bar{p}^{(1)}\delta_{ij}+2\bar{E}_{ij}^{(1)}+(1-\beta)\bar{M}_{ij} \tag{B.4}$$

$$\bar{M}_{ij}\equiv-2\bar{u}_k^{(0)}\nabla_k\bar{E}_{ij}^{(0)}+\nabla_k\bar{u}_i^{(0)}\bar{E}_{jk}^{(0)}+\nabla_k\bar{u}_j^{(0)}\bar{E}_{ik}^{(0)} \tag{B.5}$$

The *Giesekus Equation* (Bird, Equation 6.3-6) [21] is equivalent to the following:

$$2\nabla_j\left[\bar{u}_k^{(0)}\nabla_k\bar{E}_{ij}^{(0)}-\nabla_k\bar{u}_i^{(0)}\bar{E}_{jk}^{(0)}-\nabla_k\bar{u}_j^{(0)}\bar{E}_{ik}^{(0)}\right] \tag{B.6}$$

$$=-4\nabla_j\bar{E}_{ik}^{(0)}\bar{E}_{kj}^{(0)}+\nabla_i\left[\frac{D}{Dt}\bar{p}^{(0)}+\bar{E}_{jk}^{(0)}\bar{E}_{jk}^{(0)}\right] \tag{B.7}$$

$$\therefore \nabla_j \bar{M}_{ij} = -\nabla_j \left[2\bar{E}^{\nabla(0)}_{ij} \right] = \nabla_j \left[4\bar{E}^{(0)}_{ik} \bar{E}^{(0)}_{kj} \right] - \nabla_i \left[\frac{D}{Dt}\bar{p}^{(0)} + \bar{E}^{(0)}_{jk} \bar{E}^{(0)}_{jk} \right] \tag{B.8}$$

We can rewrite the divergence of $\bar{M}_{ij}$ as equal to the divergence of another tensor G_{ij} such that:

$$\nabla_j \bar{M}_{ij} = \nabla_j G_{ij} \tag{B.9}$$

$$G_{ij} \equiv -\bar{E}^{(0)}_{kl} \bar{E}^{(0)}_{kl} \delta_{ij} + 4\bar{E}^{(0)}_{ik} \bar{E}^{(0)}_{kj} \tag{B.10}$$

We want to relate this to the reciprocal theorem, which shows the propulsion occurs from the following integral over V_f, the fluid domain exterior to the swimmer:

$$U^{(1)}_i F^{\text{aux}}_i - U^{\text{aux}}_i F^{(1)}_i = (1-\beta) \int_{V_f} \nabla_j u^{\text{aux}}_i \bar{M}_{ij} \, dV \tag{B.11}$$

Consider the following integrals involving $\bar{M}_{ij}$ and G_{ij}

$$\int_{V_f} \nabla_j u^{\text{aux}}_i \bar{M}_{ij} \, dV = \int_{V_f} \nabla_j (u^{\text{aux}}_i \bar{M}_{ij}) \, dV - \int_{V_f} u^{\text{aux}}_i \nabla_j \bar{M}_{ij} \, dV \tag{B.12}$$

$$= -\int_S u^{\text{aux}}_i \bar{M}_{ij} n_j \, dA - \int_{V_f} u^{\text{aux}}_i \nabla_j \bar{M}_{ij} \, dV \tag{B.13}$$

$$\int_{V_f} \nabla_j u^{\text{aux}}_i G_{ij} \, dV = \int_{V_f} \nabla_j (u^{\text{aux}}_i G_{ij}) \, dV - \int_{V_f} u^{\text{aux}}_i \nabla_j \bar{M}_{ij} \, dV \tag{B.14}$$

$$= -\int_S u^{\text{aux}}_i G_{ij} n_j \, dA - \int_{V_f} u^{\text{aux}}_i \nabla_j G_{ij} \, dV \tag{B.15}$$

The two surface integrals can be converted to volume integrals over the interior of the swimmer V_S, which is undergoing rigid rotation (at zero-th order in De). Since the tensors $\bar{M}_{ij}$, G_{ij} comprise entirely of terms involving the *rate-of-strain tensor*, which is zero in a rigidly rotating domain, these integrals evaluate to zero.

$$\int_{V_f} \nabla_j u^{\text{aux}}_i \bar{M}_{ij} \, dV = -U^{\text{aux}}_i \cancelto{0}{\int_{V_S} \nabla_j \bar{M}_{ij} \, dV} - \int_{V_f} u^{\text{aux}}_i \nabla_j \bar{M}_{ij} \, dV \tag{B.16}$$

$$\int_{V_f} \nabla_j u^{\text{aux}}_i G_{ij} \, dV = -U^{\text{aux}}_i \cancelto{0}{\int_{V_S} \nabla_j G_{ij} \, dV} - \int_{V_f} u^{\text{aux}}_i \nabla_j G_{ij} \, dV \tag{B.17}$$

The Giesekus equation also shows the last term in each of the above two equations are equal. Hence:

$$\int_{V_f} \nabla_j u^{\text{aux}}_i \bar{M}_{ij} \, dV = \int_{V_f} \nabla_j u^{\text{aux}}_i G_{ij} \, dV \tag{B.18}$$

$$= \int_{V_f} \nabla_j u^{\text{aux}}_i (4\bar{E}^{(0)}_{ik} \bar{E}^{(0)}_{kj}) \, dV \tag{B.19}$$

$$\therefore \int_{V_f} \nabla_j u^{\text{aux}}_i \bar{M}_{ij} \, dV = \int_{V_f} \nabla_j u^{\text{aux}}_i (\bar{\sigma}^{p(0)}_{ik} \bar{\sigma}^{p(0)}_{kj}) \, dV \tag{B.20}$$

This is helpful for compactness, but especially also because the square of the zero-th order polymer stress shows up in the Giesekus constitutive equation. For instance, when the Giesekus α parameter is non-zero:

$$\bar{\sigma}^{(1)}_{ij} = -\bar{p}^{(1)} \delta_{ij} + 2\bar{E}^{(1)}_{ij} + (1-\beta) \left[\bar{M}_{ij} - \alpha \bar{\sigma}^{p(0)}_{ik} \bar{\sigma}^{p(0)}_{kj} \right] \tag{B.21}$$

$$U^{(1)}_i F^{\text{aux}}_i - U^{\text{aux}}_i F^{(1)}_i = (1-\beta) \int_{V_f} \nabla_j u^{\text{aux}}_i \left[\bar{M}_{ij} - \alpha \bar{\sigma}^{p(0)}_{ik} \bar{\sigma}^{p(0)}_{kj} \right] dV \tag{B.22}$$

$$= (1-\beta)(1-\alpha) \int_{V_f} \nabla_j u^{\text{aux}}_i \bar{\sigma}^{p(0)}_{ik} \bar{\sigma}^{p(0)}_{kj} \, dV \tag{B.23}$$

This demonstrates clearly the linearity of the steady swimmer translational velocity in $(1-\beta)(1-\alpha)$

Appendix C. General transient solution via convolution

We consider a freely-suspended swimmer, with a non-dimensional tail rotation rate whose magnitude varies with time as $\Gamma(t)$ and orientation $\hat{\Omega}_i$ remains unchanged. This leads to the following boundary conditions:

$$p(r \to \infty) \to 0 \tag{C.1}$$

$$u_i(|x_i| \to \infty) \to 0 \tag{C.2}$$

$$u^0_i(x^s_i) = \Gamma(t) \epsilon_{ijk} \hat{\Omega}_j x^s_k \qquad \forall \, x^s_i \text{ on surface} \tag{C.3}$$

C.1. Zero-th order solution for pressure, velocity, and polymer stress

We apply a Fourier transform to convert the time-domain variable t to the frequency domain variable k, using carets to denote variables in the frequency domain. Due to orthogonality, the space-domain components remain unchanged. Applying the Fourier transform to the system zero-th order, the governing equations and boundary conditions are as follows:

$$0 = -\nabla_i \hat{p}^{(0)} + \beta \nabla^2 \hat{u}^{(0)}_i + (1-\beta) \nabla_j \hat{\sigma}^{p(0)}_{ij} \tag{C.4}$$

$$\nabla_i \hat{u}^{(0)}_i = 0 \tag{C.5}$$

$$\hat{u}^0_i|_{\text{surface}} = \hat{\Gamma}(k) \epsilon_{ijk} p_j r_k \tag{C.6}$$

$$(ik+1) \hat{\sigma}^{(0)}_{ij} = 2E^{(0)}_{ij} \tag{C.7}$$

We assume the variables are separable into the product of spatial and time dependencies, with the spatially-varying components denoted by overbars. From the velocity boundary condition, the zero-th order velocity, and subsequently polymer stress, can be determined:

$$\hat{u}^0_i = \hat{\Gamma} \bar{u}^0_i \tag{C.8}$$

$$\hat{\sigma}^{p(0)}_{ij} = \frac{\hat{\Gamma}}{1+ik} \bar{\sigma}^{p(0)}_{ij} \tag{C.9}$$

$$= \frac{\hat{\Gamma}}{1+ik} (2\bar{E}^{(0)}_{ij}) \tag{C.10}$$

The Stokes equation at zero-th order is hence:

$$\nabla_i \hat{p}^{(0)} = \left[\beta \hat{\Gamma} + \frac{(1-\beta)\hat{\Gamma}}{1+ik} \right] \nabla^2 \bar{u}^{(0)}_i \tag{C.11}$$

Isolating the spatial components for the pressure and velocity in the above equation:

$$\hat{p}^{(0)} = \left[\beta \hat{\Gamma} + \frac{(1-\beta)\hat{\Gamma}}{1+ik} \right] \bar{p}^{(0)} \tag{C.12}$$

$$\nabla_i \bar{p}^{(0)} = \nabla^2 \bar{u}^{(0)}_i \tag{C.13}$$

This shows the spatial components of the zero-th order pressure and velocity correspond to the Newtonian Stokes solutions. Due to reversibility of Stokes flow, no propulsion is created at this order. Further, because the Newtonian problem is for an axisymmetric body rotating in a Newtonian quiescent fluid, no pressure is generated and $p^{(0)}$ is identically zero [25].

$$p^{(0)} = 0 \tag{C.14}$$

C.2. Linear order solution for pressure, velocity, and polymer stress

To apply the Fourier transform to products of time-dependent terms in Eq. (27), the convolution theorem results in convolutions of frequency-dependent terms after applying the transform. Hence we define new terms for ease of notation:

$$\hat{\Gamma}_{n1} = \hat{\Gamma} * \frac{\hat{\Gamma}}{1+ik} \tag{C.15}$$

$$\hat{\Gamma}_{n2} = \frac{\hat{\Gamma}}{1+ik} * \frac{\hat{\Gamma}}{1+ik} \tag{C.16}$$

Here, the $*$ indicates convolution between the two functions. The Fourier-transformed governing equations and boundary conditions at linear order are hence:

$$0 = -\nabla_i \hat{p}^{(1)} + \beta \nabla^2 \hat{u}^{(1)}_i + (1-\beta) \nabla_j \hat{\sigma}^{p(1)}_{ij} \tag{C.17}$$

$$\nabla_i \hat{u}_i^{(1)} = 0 \tag{C.18}$$

$$(ik+1)\hat{\sigma}_{ij}^{(1)} = \hat{\Gamma}_{n1}\bar{M}_{ij} - \alpha\hat{\Gamma}_{n2}\bar{\sigma}_{ik}^{p(0)}\bar{\sigma}_{kj}^{p(0)} + 2\hat{E}_{ij}^{(1)} \tag{C.19}$$

$$\bar{M}_{ij} = -\bar{u}_k^{(0)}\nabla_k\bar{\sigma}_{ij}^{p(0)} + \nabla_k\bar{u}_i^{(0)}\bar{\sigma}_{jk}^{p(0)} + \nabla_k\bar{u}_j^{(0)}\bar{\sigma}_{ik}^{p(0)} \tag{C.20}$$

We assume $\hat{p}^1, \hat{u}_i^1$ are separable into frequency and spatial dependencies, and obtain an expression for the linear-order polymer stress:

$$u_i^{(1)} = \hat{T}_u^1(k)\bar{u}_i^{(1)}(x_i);\ \hat{E}_{ij}^{(1)} = \hat{T}_u^1(k)\bar{E}_{ij}^{(1)} \tag{C.21}$$

$$\hat{p}^{(1)} = \hat{T}_p^1(k)\bar{p}^{(1)}(x_i) \tag{C.22}$$

$$\hat{\sigma}_{ij}^{p(1)} = \frac{\hat{\Gamma}_{n1}}{(1+ik)}\bar{M}_{ij} - \alpha\frac{\hat{\Gamma}_{n2}}{(1+ik)}\bar{\sigma}_{ik}^{p(0)}\bar{\sigma}_{kj}^{p(0)} + \frac{\hat{T}_u^1}{1+ik}(2\bar{E}_{ij}^{(1)}) \tag{C.23}$$

Substituting these fields into the Stokes equation at this order (Eq. (C.17)):

$$\hat{T}_p^1\nabla_i\bar{p}^1 = \hat{T}_u^1\left[\beta + \frac{(1-\beta)}{1+ik}\right]\nabla^2\bar{u}_i^1 + \frac{\hat{\Gamma}_{n1}}{(1+ik)}(1-\beta)\nabla_j\bar{M}_{ij} \tag{C.24}$$

$$- \frac{\alpha\hat{\Gamma}_{n2}}{(1+ik)}(1-\beta)\nabla_j\bar{\sigma}_{ik}^{p(0)}\bar{\sigma}_{kj}^{p(0)} \tag{C.25}$$

Using the identity provided by equation 6.3-6 in Bird [21], (referred to therein as the Giesekus equation) to simplify $\nabla_j\bar{M}_{ij}$:

$$\hat{T}_p^1\nabla_i\bar{\mathcal{P}}^1 = \hat{T}_u^1\left[\frac{1+i\beta k}{1+ik}\right]\nabla^2\bar{u}_i^1 \tag{C.26}$$

$$+ \frac{\hat{\Gamma}_{n1} - \alpha\hat{\Gamma}_{n2}}{(1+ik)}(1-\beta)\nabla_j\bar{\sigma}_{ik}^{p(0)}\bar{\sigma}_{kj}^{p(0)} \tag{C.27}$$

$$\bar{\mathcal{P}}^1 \equiv \bar{p}^1 + (1-\beta)\bar{E}_{jk}^{(0)}\bar{E}_{jk}^{(0)} \tag{C.28}$$

We wish to obtain $\hat{T}_u^1(k)$, which, upon transforming back into the time-domain, gives the time-dependence for the freely-suspended swimmer translational velocity. We compare the above equations to the steady equation at this order, which determines the spatial fields; i.e. $\bar{u}_i^{(1)}, \bar{p}^{(1)}$ satisfy:

$$\nabla_i\bar{\mathcal{P}}^1 = \nabla^2\bar{u}_i^1 + (1-\beta)(1-\alpha)\nabla_j\bar{\sigma}_{ik}^{p(0)}\bar{\sigma}_{kj}^{p(0)} \tag{C.29}$$

The ratio of the coefficients of each term between the two equations must be equal to satisfy Eq. (C.17):

$$\hat{T}_u^1\left[\frac{1+i\beta k}{1+ik}\right] = \frac{\hat{\Gamma}_{n1} - \alpha\hat{\Gamma}_{n2}}{(1+ik)(1-\alpha)} \tag{C.30}$$

$$\hat{T}_u^1 = \frac{\hat{\Gamma}_{n1} - \alpha\hat{\Gamma}_{n2}}{(1+i\beta k)(1-\alpha)} \tag{C.31}$$

This also gives the time-dependence of the pressure:

$$\hat{T}_p^1 = \frac{\hat{\Gamma}_{n1} - \alpha\hat{\Gamma}_{n2}}{(1+ik)(1-\alpha)} \tag{C.32}$$

Finally, for the time-dependence of the translational velocity of the freely-suspended swimmer – the key experimental observable – we need to find $T_u^1 = \mathcal{F}^{-1}[\hat{T}_u^1]$. Using the convolution theorem to simplify these expression, we obtain:

$$T_u^1(t) = \frac{1}{1-\alpha}\left(\Gamma(t)\left[\Gamma(t) * e^{-t}\right] - \alpha\left[\Gamma(t) * e^{-t}\right]^2\right) * \frac{e^{-t/\beta}}{\beta} \tag{C.33}$$

Appendix D. Complex velocity in a multi-mode fluid

We now have n Oldroyd-B modes, where the qth mode σ_{ij}^q has viscosity η and relaxation time λ_q. For each mode, we nondimensionalize its evolution equation, using the stress scale $\eta_p\tilde{\Omega}_T$ and the longest relaxation time λ_1. The following non-dimensional equations for each polymer mode arise:

$$\kappa_q\frac{\partial\sigma_{ij}^q}{\partial t} + \sigma_{ij}^q = \kappa_q\mathrm{De}_1 M_{ij}^q + 2E_{ij} \tag{D.1}$$

$$M_{ij}^q = -u_k\nabla_k\sigma_{ij}^q + \nabla_k u_i\sigma_{jk}^q + \nabla_k u_j\sigma_{ik}^q \tag{D.2}$$

$$\kappa_q \equiv \frac{\lambda_q}{\lambda_1} \tag{D.3}$$

We apply the perturbation expansion described in Section 2 to each mode up to $\mathcal{O}(\mathrm{De}^1)$. At $\mathcal{O}(1)$:

$$u_i^0 = \bar{u}_i^{(0)}\left(1 + \varepsilon e^{i\omega_1 t}\right) \tag{D.4}$$

$$\kappa_q\frac{\partial\sigma_{ij}^{q(0)}}{\partial t} + \sigma_{ij}^{q(0)} = 2\bar{E}_{ij}^{(0)}\left(1 + \varepsilon e^{i\omega_1 t}\right) \tag{D.5}$$

$$\sigma_{ij}^{q(0)} = 2\bar{E}_{ij}^{(0)}\left(1 + \frac{\varepsilon}{1+i\kappa_q\omega_1}e^{i\omega_1 t}\right) \tag{D.6}$$

Observe that $\kappa_q\omega_1 = \lambda_q\omega$, the non-dimensional oscillation frequency for the qth mode. As before, the spatial components of the zero-th order pressure and velocity correspond to the Newtonian Stokes solutions, no propulsion is created at this order, and $p^{(0)}$ is identically zero.

Next, at $\mathcal{O}(\mathrm{De})$:

$$\frac{\partial\sigma_{ij}^{q(1)}}{\partial t} + \sigma_{ij}^{q(1)} = 2E_{ij}^{(1)} + \kappa_q M_{ij}^q \tag{D.7}$$

$$= 2E_{ij}^{(1)} + \kappa_q\left(1 + \varepsilon e^{i\omega_1 t}\right)\left(1 + \frac{\varepsilon}{1+i\kappa_q\omega_1}\right)\bar{M}_{ij}^q \tag{D.8}$$

$$= 2(1 + f e^{i\omega_1 t})\bar{E}_{ij}^{(1)} + \kappa_q\left(1 + \frac{\varepsilon(2+i\kappa_q\omega_1)}{1+i\kappa_q\omega_1}\right)\bar{M}_{ij}^q \tag{D.9}$$

$$\sigma_{ij}^{q(1)} = 2(1 + \frac{f}{1+i\kappa_q\omega_1}e^{i\omega_1 t})\bar{E}_{ij}^{(1)} + \kappa_q\left(1 + \frac{\varepsilon(2+i\kappa_q\omega_1)}{(1+i\kappa_q\omega_1)^2}\right)\bar{M}_{ij}^q \tag{D.10}$$

As in Section 2.2.2, we give $E_{ij}^{(1)}$ a time dependence $1 + f e^{i\omega_1 t}$, and we give $p^{(1)}$ the time dependence $1 + g e^{i\omega_1 t}$. Comparing the steady and transient components and noting that and $M_{ij}^q = M_{ij}$ for all modes:

$$\nabla_i\bar{p}^{(1)} = \beta\nabla^2\bar{u}_i^{(1)} + \sum_{q=1}^n \beta_q\nabla_j\sigma_{ij}^{q(1)} \tag{D.11}$$

$$= \beta\nabla^2\bar{u}_i^{(1)} + \sum_{q=1}^n \beta_q\nabla_j(2E_{ij}^{(1)}) + \sum_{q=1}^n \beta_q\kappa_q\nabla_j M_{ij}^q \tag{D.12}$$

$$= \nabla^2\bar{u}_i^{(1)} + \nabla_j M_{ij}\sum_{q=1}^n \beta_q\kappa_q \tag{D.13}$$

Now we examine the sinusoidal terms in the multimode and compare coefficients:

$$g\nabla_i\bar{p}^{(1)} = \nabla^2\bar{u}_i^{(1)}\left[\beta f + \sum_{q=1}^n \frac{\beta_q}{1+i\kappa_q\omega_1}\right] + \nabla_j M_{ij}\sum_{q=1}^n \beta_q\kappa_q\frac{\varepsilon(2+i\kappa_q\omega_1)}{(1+i\kappa_q\omega_1)^2} \tag{D.14}$$

As we are interested in the ratio of the oscillating velocity to the steady velocity, we rescale the coefficient of the M_{ij} term such that the steady Eq. (D.13) can be directly compared to the unsteady equation:

$$[g]\left\{\nabla_i\bar{p}^{(1)}\right\} = \left\{\nabla^2\bar{u}_i^{(1)}\right\}\left[\beta f + \sum_{q=1}^n \frac{\beta_q f}{1+i\kappa_q\omega_1}\right] \tag{D.15}$$

$$+ \left\{\nabla_j M_{ij}\sum_{q=1}^n \beta_q\kappa_q\right\}\left[\frac{\sum_{q=1}^n \beta_q\kappa_q\frac{\varepsilon(2+i\kappa_q\omega_1)}{(1+i\kappa_q\omega_1)^2}}{\sum_{q=1}^n \beta_q\kappa_q}\right] \tag{D.16}$$

Above, terms in curly braces match (D.13) and thus the time-dependence of the pressure and velocity can be recovered by comparing only the terms in square braces:

$$g = \frac{\sum_{q=1}^n \beta_q\kappa_q\frac{\varepsilon(2+i\kappa_q\omega_1)}{(1+i\kappa_q\omega_1)^2}}{\sum_{q=1}^n \beta_q\kappa_q} \tag{D.17}$$

$$\beta f + \sum_{q=1}^n \frac{\beta_q f}{1+i\kappa_q\omega_1} = \frac{\sum_{q=1}^n \beta_q\kappa_q\frac{\varepsilon(2+i\kappa_q\omega_1)}{(1+i\kappa_q\omega_1)^2}}{\sum_{q=1}^n \beta_q\kappa_q} \tag{D.18}$$

$$f = \left[\beta + \sum_{q=1}^n \frac{\beta_q}{1+i\kappa_q\omega_1}\right]^{-1}\frac{\sum_{q=1}^n \beta_q\kappa_q\frac{\varepsilon(2+i\kappa_q\omega_1)}{(1+i\kappa_q\omega_1)^2}}{\sum_{q=1}^n \beta_q\kappa_q} \tag{D.19}$$

This complex prefactor f is thus the complex velocity of a swirler in a multi-mode Oldroyd-B fluid.

References

[1] E.M. Purcell, Life at low Reynolds number, Am. J. Phys. 45 (1) (1977) 3–11.
[2] E. Lauga, T.R. Powers, The hydrodynamics of swimming microorganisms, Rep. Progr. Phys. 72 (9) (2009) 096601.
[3] A. Shapere, F. Wilczek, Geometry of self-propulsion at low Reynolds number, J. Fluid Mech. 198 (1989) 557–585.
[4] T. Qiu, T.-C. Lee, A.G. Mark, K.I. Morozov, R. Münster, O. Mierka, S. Turek, A.M. Leshansky, P. Fischer, Swimming by reciprocal motion at low Reynolds number, Nat. Commun. 5 (1) (2014) 5119.
[5] T. Qiu, S. Palagi, P. Fischer, 3D-printed soft microrobot for swimming in biological fluids, in: 2015 37th Annual International Conference of the IEEE Engineering in Medicine and Biology Society, EMBC, IEEE, 2015, pp. 4922–4925.
[6] T. Normand, E. Lauga, Flapping motion and force generation in a viscoelastic fluid, Phys. Rev. E 78 (6) (2008) 061907.
[7] C. Datt, B. Nasouri, G.J. Elfring, Two-sphere swimmers in viscoelastic fluids, Phys. Rev. Fluids 3 (12) (2018) 123301.
[8] K. Yasuda, M. Kuroda, S. Komura, Reciprocal microswimmers in a viscoelastic fluid, Phys. Fluids 32 (9) (2020).
[9] M. Eberhard, A. Choudhary, H. Stark, Why the reciprocal two-sphere swimmer moves in a viscoelastic environment, Phys. Fluids 35 (6) (2023).
[10] L.W. Rogowski, J. Ali, X. Zhang, J.N. Wilking, H.C. Fu, M.J. Kim, Symmetry breaking propulsion of magnetic microspheres in nonlinearly viscoelastic fluids, Nat. Commun. 12 (1) (2021) 1116.
[11] O.S. Pak, L. Zhu, L. Brandt, E. Lauga, Micropropulsion and microrheology in complex fluids via symmetry breaking, Phys. Fluids 24 (10) (2012) 103102.
[12] J.A. Puente-Velázquez, F.A. Godínez, E. Lauga, R. Zenit, Viscoelastic propulsion of a rotating dumbbell, Microfluid. Nanofluid. 23 (2019) 1–7.
[13] L.W. Rogowski, H. Kim, X. Zhang, M.J. Kim, Microsnowman propagation and robotics inside synthetic mucus, in: 2018 15th International Conference on Ubiquitous Robots, UR, IEEE, 2018, pp. 5–10.
[14] J.P. Binagia, E.S.G. Shaqfeh, Self-propulsion of a freely suspended swimmer by a swirling tail in a viscoelastic fluid, Phys. Rev. Fluids 6 (2021) 053301, http://dx.doi.org/10.1103/PhysRevFluids.6.053301, URL https://link.aps.org/doi/10.1103/PhysRevFluids.6.053301.
[15] L. Kroo, J.P. Binagia, N. Eckman, M. Prakash, E.S. Shaqfeh, A freely suspended robotic swimmer propelled by viscoelastic normal stresses, J. Fluid Mech. 944 (2022) A20.
[16] K.D. Housiadas, R.I. Tanner, A high-order perturbation solution for the steady sedimentation of a sphere in a viscoelastic fluid, J. Non-Newton. Fluid Mech. 233 (2016) 166–180.
[17] G.H. McKinley, Steady and transient motion of spherical particles in viscoelastic liquids, Transp. Process. Bubble Drops Particles (2002) 338–375.
[18] M.N. Moore, M.J. Shelley, A weak-coupling expansion for viscoelastic fluids applied to dynamic settling of a body, J. Non-Newton. Fluid Mech. 183 (2012) 25–36.
[19] M.A. Joens, J.W. Swan, Unsteady and lineal translation of a sphere through a viscoelastic fluid, Phys. Rev. Fluids 7 (1) (2022) 013301.
[20] M.A. Joens, P.S. Doyle, G.H. McKinley, J.W. Swan, Time-dependent two-dimensional translation of a freely rotating sphere in a viscoelastic fluid, Phys. Fluids 34 (12) (2022).
[21] R.B. Bird, R.C. Armstrong, O. Hassager, Dynamics of polymeric liquids, in: Fluid mechanics, vol. 1, John Wiley and Sons Inc., New York, NY, 1987.
[22] G.J. Elfring, E. Lauga, Theory of locomotion through complex fluids, Complex Fluids Biol. Syst. Exper. Theory Comput. (2015) 283–317.
[23] K.D. Housiadas, R.I. Tanner, The angular velocity of a freely rotating sphere in a weakly viscoelastic matrix fluid, Phys. Fluids 23 (5) (2011) 051702.
[24] J.G. Oldroyd, On the formulation of rheological equations of state, Proc. R. Soc. London. Series A 200 (1063) (1950) 523–541.
[25] E. Guazzelli, J.F. Morris, A Physical Introduction To Suspension Dynamics, Vol. 45, Cambridge University Press, 2011.
[26] R. Fattal, R. Kupferman, Constitutive laws for the matrix-logarithm of the conformation tensor, J. Non-Newton. Fluid Mech. 123 (2–3) (2004) 281–285.
[27] M.A. Hulsen, R. Fattal, R. Kupferman, Flow of viscoelastic fluids past a cylinder at high weissenberg number: stabilized simulations using matrix logarithms, J. Non-Newton. Fluid Mech. 127 (1) (2005) 27–39.
[28] C.G. Broyden, A class of methods for solving nonlinear simultaneous equations, Math. Comput. 19 (92) (1965) 577–593.
[29] P.E. Rouse Jr., A theory of the linear viscoelastic properties of dilute solutions of coiling polymers, J. Chem. Phys. 21 (7) (1953) 1272–1280.
[30] L.G. Leal, Advanced Transport Phenomena: Fluid Mechanics and Convective Transport Processes, Vol. 7, Cambridge University Press, 2007.